Viscoelastic flow past a confined cylinder of a polyisobutylene solution

Viscoelastic flow past a confined cylinder of a polyisobutylene solution

Hans P. W. Baaijens,[a),b)] Gerrit W. M. Peters, Frank P. T. Baaijens,

and Han E. H. Meijer

Center for Polymers and Composites, Eindhoven University of Technology, P.O. Box 513, 5600 MB Eindhoven, The Netherlands

(Received 30 May 1995; accepted 18 July 1995)

Synopsis

Viscoelastic constitutive equations are evaluated using the benchmark problem of the planar flow past a confined cylinder for a well-characterized solution of 5%(w/w) polyisobutylene in tetradecane. The ratio of channel height to cylinder diameter is equal to two. We compare finite element simulations with point-wise measured velocities and stresses obtained by means of laser Doppler anemometry and a flow-induced birefringence technique, respectively. The Deborah number (De) ranges from 0.25 to 2.32. In the case of the geometry with a symmetrically confined cylinder, computations were made with a generalized Newtonian model and with both a single- and a four-mode Phan-Thien and Tanner (PTT) model. All model parameters were determined in simple shear flow. A similar analysis is presented in case of an asymmetrically confined cylinder (with De = 1.87). Impressively good agreement was found between the predictions of the four-mode PTT model and the measured velocities and stresses. The agreement was even excellent in the geometry with the asymmetrically confined cylinder. © *1995 Society of Rheology.*

I. INTRODUCTION

A. Motivation

The quality of viscoelastic flow simulations in complex geometries, i.e., where mixed shear and elongational deformation occur, depends strongly on the adequacy of the constitutive equation used to describe the non-Newtonian behavior of the polymeric liquid.

In rheology, it is customary to evaluate constitutive equations in simple shear flows (viscometric flows). However, as is well known now, for two reasons such flows do not contain enough information concerning the fluid rheology to ensure reliable predictions in more complex flows. First, in many cases the viscometric functions can only be measured in a range of shear rates that is smaller than the range present in the actual practical flow. Second, and more essential, complex flows involve both shear and elongational deformation. Unfortunately, measurements of material functions in purely elongational flows are often unreliable or even impossible [Walters (1992)]. Therefore it is generally acknowledged that, apart from simple shear flows, *complex flows* should be used to find the (parameters of) constitutive equations for (polymeric) viscoelastic liquids.

[a)]Present address: Philips Research, Prof. Holstlaan 4, 5656 AA Eindhoven, The Netherlands.
[b)]Corresponding author.

In the past two decades, numerous viscoelastic constitutive equations have been proposed for polymeric liquids [see, for example, Bird *et al.* (1987) and Larson (1988)]. With the development of new reliable numerical techniques, simulations with these equations can be made presently in a reasonable range of complex flows [see, for example, Brown and McKinley (1994)] and the results can be compared with experimental data. In future work, the measured data in complex flows may be used to improve the fit of the model parameters.

B. History of the subject

A vast number of papers on complex polymer flows exist. Four basic types of those flows studied in literature can be distinguished: rotational flows (such as the flow between two eccentric rotating cylinders), contraction flows (in particular the four to one contraction), stagnation flows (flows past obstacles, e.g., spheres and cylinders), and free surface flows ["die (extrudate) swell"]. The contraction flows have received by far the most interest and for comprehensive reviews one is referred to Boger (1987) and Quinzani (1991).

Numerous numerical methods have been developed for computing viscoelastic flows at higher Deborah numbers (De $>$ 1). Recently, it was shown for the benchmark problem of a sphere falling in a tube, using an upper convected Maxwell (UCM) fluid, that widely varying methods yield the same answers [Brown and McKinley (1994)]. This important result gives confidence that numerical solutions are true solutions of the mathematical problem and that no additional uncertainties are introduced.

Experimental methods commonly used are streak-line visualization with tracer particles and laser Doppler anemometry (LDA) for measuring the velocity field on the one hand and flow-induced birefringence (FIB) for stress measurements on the other.

LDA has been used mostly in the case of polymer solutions (e.g., Davidson *et al.* (1993a), Davidson *et al.* (1993b), Aldhouse *et al.* (1986), Quinzani *et al.* (1994), Raiford *et al.* (1989).

Stress measurements are based on flow-induced birefringence, using the linear stress optical rule (SOR). In polymer melts, it is fairly easy to measure the birefringence with, for example, the crossed polarizers experiment [e.g., Aldhouse *et al.* (1986), Han and Drexler (1973a), Han and Drexler (1973b), Han and Drexler (1973c), Isayev and Upadhyay (1985), Kajiwara *et al.* (1993), Kiriakidis *et al.* (1993), Maders *et al.* (1992), White and Baird (1988)].

In the case of polymer solutions the birefringence is so small that more sensitive measurement techniques are required. An example is the rheo-optical analyzer (ROA) developed by Fuller and Mikkelsen (1989). [Fuller (1995) gives a comprehensive review of techniques to measure birefringence.] The use of techniques like ROA in complex flows is not widespread yet, although some studies exist: Davidson *et al.* (1993a), Davidson *et al.* (1993b), Galante and Fratini (1993), Quinzani *et al.* (1994), and Rajagopalan *et al.* (1992). Both LDA and ROA have the advantage of measuring data point-wise: together they enable the most quantitative mapping of both velocity and stress field.

Studies that combined point-wise velocity and stress measurements are rare. Quinzani (1991), Quinzani *et al.* (1994) and Armstrong *et al.* (1992) studied in this way the flow of a polyisobutylene solution through a planar four to one contraction. Davidson *et al.* (1993a) and Davidson *et al.* (1993b) similarly studied the flow of a polystyrene solution through a planar wavy walled channel. Both groups, however, did not compare their experimental data with complete numerical simulations using viscoelastic constitutive equations. In the study of Quinzani (1991) stresses were computed along the centerline only by means of integration of viscoelastic constitutive equations using the measured

velocity field. They tested various constitutive equations by comparing the computed results with the measured stresses. Though this procedure rapidly provides information on the quality of viscoelastic constitutive equations, it has one major drawback, since it is not guaranteed that the computed stresses and measured velocities are consistent with the solution of the full fluid mechanical problem. Mitsoulis (1993) found reasonable overall agreement between numerical simulations for an integral model of the K-BKZ type with the experimental data of Quinzani (1991). However, he overpredicts the stresses by as much as 40% for the highest Deborah numbers ($De \leq 0.77$).

A second attempt to compare both point-wise measured stress and velocity data with numerical simulations in a complex flow is reported in our previous paper Baaijens *et al.* (1994). That study concerned the flow of a polyisobutylene solution (as used by Quinzani *et al.*) in the planar flow past a symmetrically confined cylinder at a low Deborah number ($De = 0.22$). Surprisingly, we found a dramatic discrepancy between measured and computed stresses downstream of the cylinder along the centerline. The measured stresses reached a maximum that was a factor of 2 higher than computed. Even more dramatically, the measured stresses relaxed much slower: at the centerline after seven cylinder radii, the measured stresses were about 50% of their maximum value, while in the computations stresses were fully relaxed to zero after five radii. These results came up in three independent experiments (with the same batch of fluid). These findings induced the present study in which we build a new experimental apparatus to study the same flow over a wider range of Deborah numbers.

Before elucidating the objectives of the present study in more detail, related literature on flows of polymer solutions past cylinders is reviewed first. It is found for polymer solutions that the effect of viscoelasticity on the velocity field is influenced by (i) the position of the constraining walls, (ii) by the degree of elasticity in the flow (characterized by the Deborah number), (iii) by the relative importance of inertia (characterized by the Reynolds number), and (iv) by the rheological behavior of the liquid in elongational flow.

In case of the *unbounded* flow past a cylinder (in a uniform stream, i.e., with a uniform velocity field far from the cylinder) experiments gave only a small effect of viscoelasticity on the streamline pattern [Manero and Mena (1981), Mena and Caswell (1974), Ultmann and Denn (1970)]. The results seemed contradictory: the streamlines shifted either a little upstream or downstream of the cylinder relative to the Newtonian flow situation. Based on their experimental results, Manero and Mena (1981) suggested that the direction depends on the value of the De number: a downstream shift at low elasticity ($De < 1$) and an upstream shift at high elasticity ($De > 1$).

Two early full numerical studies that solved the planar flow past a cylinder in a uniform stream have been reported. Pilate and Crochet (1977) applied a second-order fluid model at low to moderate Deborah numbers ($0 < De < 1$) and low to high Reynolds numbers ($0.1 < Re < 100$). Townsend (1980) considered two Oldroyd models (one representing a constant viscosity, elastic fluid, and one representing a viscoelastic fluid with shear thinning) at low Deborah numbers. Both studies revealed a small downstream displacement of the streamlines as observed experimentally by Manero and Mena (1981).

The flow past a *symmetrically confined* cylinder has not been studied extensively. Dhahir and Walters (1989) reported some experiments and calculations, but focused merely on the eccentric case which will be discussed below. McKinley (1991) reported unique LDA measurements of flow instabilities past a symmetrically confined cylinder, using an organic Boger fluid. Further, we already mentioned our previous study Baaijens *et al.* (1994).

In the case of the *asymmetrically confined* cylinder, the effect of viscoelasticity on the velocity field is more pronounced. This is explained by the influence of the stress field on the kinematics. The effect is demonstrated experimentally by Walters and coworkers [Dhahir and Walters (1989), Cochrane *et al.* (1981), Jones and Walters (1989), Georgiou *et al.* (1991)]. Cochrane *et al.* (1981) observed that the streak lines for a viscoelastic fluid were much more sensitive for a small asymmetry in the constraining of the cylinder than for a purely viscous, Newtonian fluid. Dhahir and Walters (1989) visualized streamlines for the planar flow past an asymmetrically confined cylinder and observed that for a (elongational thickening) viscoelastic liquid more material flows through the broader gap, compared with a Newtonian liquid. Jones and Walters (1989) and Georgiou *et al.* (1991) found the same effect in the flow of several types of liquids through an antisymmetric array of confined cylinders. It is considered as a manifestation of the extensional viscosity: molecules entering the narrow gap must elongate more strongly than those entering the broad gap, which results, for elongational thickening liquids, in a locally higher flow resistance in the narrow gap. Interestingly, Olsson (1994) simulated with the Giesekus model the start-up of flow past a cylinder that is located near one on the walls. He found unstable behavior of the fluid, that was more pronounced if the velocity was increased and/or the velocity rise time was shortened.

To end with, the work of Liu *et al.* (1995) is of interest in this context as well. They performed experiments with spheres rolling in a viscoelastic fluid down an inclined wall and observed that the sense of the rotation is in the other direction compared with a sphere rolling down an inclined plane in a Newtonian fluid (in which case it rotates as in air). Moreover, if a sphere was dropped a small distance from a vertical wall in a viscoelastic fluid, the sphere moved to the wall and rotated in the "counter" sense. If the same sphere was dropped in a Newtonian fluid, it moved away from the wall. These effects are also explained by the reluctance of polymer molecules to flow through the narrow gap between sphere and wall. The net force on the sphere causes its counter rotation compared with a Newtonian fluid.

C. Objectives and choices made

The main objective of the present study was to evaluate viscoelastic constitutive equations by means of a comparison of point-wise measured data of both velocity and stress fields with results of numerical simulations of the complex flow.

To facilitate the analysis both experimentally and computationally, model fluids are used instead of polymer melts. The benchmark problem [Brown and McKinley (1994)] of the stagnation flow past a confined circular cylinder is used in two variations: a symmetrically and an asymmetrically confined cylinder.

Several features make this type of complex flow geometry interesting. First, it has received far less interest than contraction flows. In particular, a detailed quantitative mapping of the stress and velocity field and a comparison with numerical simulation does not exist yet for this flow.

Second, viscoelastic finite element computations are presently only feasible in two-dimensional flows. Planar flows have the advantage, compared with axisymmetric flows, that stresses can be measured with birefringence techniques. In nonplanar flows the interpretation of birefringence measurements in terms of stresses is far more complex, if not impossible.

Third, the flow past a submerged circular object differs in a fundamental way from the (almost classical) 4:1 contraction flow. On the surface of the cylinder two stagnation points exist: one at the front where the material is compressed, and one at the aft, where the material is stretched after being sheared along the side of the surface of the object.

Compared with the contraction flows, elongation rates are expected to be higher since the material is accelerated from rest in the rear stagnation point. This complex flow field is promising to contain relevant information for testing constitutive equations.

And fourth and finally, numerical simulations of abrupt contraction flows suffer from the complication of the presence of singular re-entry corner points. Such difficulties are absent in the flow past a cylinder, which is expected to facilitate the computations.

In the experiments the cylinder will be confined, since it has been observed that the effect of viscoelasticity on the velocity field is influenced by the relative position of the cylinder to the confining plates (see Sec. I B).

Velocities will be measured point-wise with laser Doppler anemometry (LDA), and stresses with a flow-induced birefringence (FIB) technique. Only a few studies have used these two methods simultaneously [Armstrong *et al.* (1992), Davidson *et al.* (1993b)]. A 5%(w/w) polyisobutylene in tetradecane solution will be used as model fluid to connect with the study of Armstrong *et al.* (1992), who analyzed experimentally in the same way the flow of the same fluid through a four to one contraction. The fluid is viscoelastic and shear thinning, which behavior is preferred when aiming at making progress towards "melt-like" behavior [Brown and McKinley (1994)].

II. METHODS

A. Fluid preparation and rheological characterization

A solution of 5%(w/w) polyisobutylene (Vistanex L120, Exxon Chem., weight average molecular weight $M_w \approx 1\times10^6$) in tetradecane ($C_{14}H_{30}$, isomeric mixture of 95% purity) was used as a model fluid, which is the same fluid as used by Quinzani *et al.* (1990) and Quinzani *et al.* (1994).

The fluid was prepared by cutting the polyisobutylene first in cubes of ≈ 0.5 cm^3. These were added in the appropriate amount to tetradecane in 1ℓ bottles, while stirring with a magnetic stirrer at ambient temperature (≈ 24 °C). After stirring during at least 5 days the bottles were rotated on a rolling machine for approximately one week to improve the homogeneity of the solution.

A Rheometrics-RFS-II viscometer with a cone-plate geometry (diameter 50 mm, cone angle 0.0199 rad) was used to characterize the rheology of the fluid in simple shear. Steady, dynamic, and transient tests have been performed. The results are presented in Sec. III A.

B. Experimental apparatus for complex flows

1. Flow loop

The experiments were performed with a closed flow loop: a rotary pump (Nakamura RO-10-VT) was used to pump continuously approximately 2.5ℓ of the solution from a glass reservoir through the flow cell and back into the reservoir. Reservoir, pump, and flow cell are connected by solvent resistant, flexible tubing (with inner walls made of Viton or NBR rubber). The flow cell is made of plexiglas (PMMA) with side windows made of Schott SF-57 glass (Schott Glass Inc.). This special glass is extremely low in birefringence (it has a stress optical coefficient that is 2×10^{-14} Pa^{-1}, roughly more than 100 times smaller than other glass types). To avoid stain formation, these special windows were coated [with an antireflection coating (TiO_2)].

2. Laser Doppler equipment

A differential Doppler technique was used in backscatter mode [Drain (1980)] to measure the velocity component U normal to the bisector of the two crossed beams (with intersection angle θ) according the equation:

$$\nu_D = \nu_{\text{shift}} + \frac{2U}{\lambda} \sin\frac{\theta}{2}, \tag{1}$$

where ν_D is the Doppler frequency that is measured by the flow velocity analyzer (Dantec 58N20), ν_{shift} is a preset frequency shift that enables to measure negative velocities, λ is,the wavelength of the light.

The measurements are operated from a personal computer with the software Floware (Dantec). The incident light beams are generated by a 300 mW argon-ion laser (Ion Laser Technology 5500A) and the green component with wavelength $\lambda = 514.5$ nm was used. The laser probe is fixed on an XYZ-traverse (Dantec, Lightweight Traverse), that is controlled by Floware. It has a range of 540 mm along each axis.

The spatial resolution of the laser Doppler measurements is determined by the dimensions of the measuring volume which has an ellipsoidal shape with dimensions $50\times50\times200$ μm in our case. The resolution of the velocity measurement is determined by the FVA hardware and amounts 0.13 mm/s.

3. FIB equipment

Birefringence techniques that use polarization modulation of light enable simultaneous and point-wise measurement of both extinction angle χ and phase retardation δ. Fuller (1990) has reviewed this subject. In the present study, the polarization modulation technique is applied that uses a rotating (with frequency ω) half-wave plate [as introduced by Fuller and Mikkelsen (1989)]. The measurement system, called rheo-optical analyzer (ROA), was provided by Fuller.

The measurement system ROA consists of a sequence of optical elements together with some computer hardware and software. Details of the whole system are described in Baaijens (1994). The optical part contains the polarization modulation generator, which consists of a laser, polarizer, and a rotating half-wave plate. Then a lens collimates the laser beam before it enters the flow cell. After the flow cell a circular polarizer and a photodetector complete the optical train. Neglecting system imperfections, the time-dependent intensity signal is described by [Fuller and Mikkelsen (1989)]

$$I = \tfrac{1}{4} I_0[1 + R_1 \sin(4\omega t) + R_2 \cos(4\omega t)], \tag{2}$$

where I_0 is the intensity at the exit of the diode laser, and R_1 and R_2 are

$$R_1 = -\sin\delta\cos 2\chi \tag{3}$$

$$R_2 = \sin\delta\sin 2\chi. \tag{4}$$

R_1 and R_2 are obtained from the measured intensity signal by means of a Fourier transformation. Since $\chi \in [-\pi/4, \pi/4]$, the angles χ and δ follow directly from Eqs. (3) and (4);

$$\chi = \arctan(-R_2/R_1), \tag{5}$$

$$\delta = \text{sign}(R_1)\arcsin\sqrt{R_1^2 + R_2^2}. \tag{6}$$

Stresses can now be found after substitution of Eqs. (5) and (6) (with birefringence $\Delta n = \lambda/(2\pi d)\delta$, d: length of light path, λ: wavelength of light) in

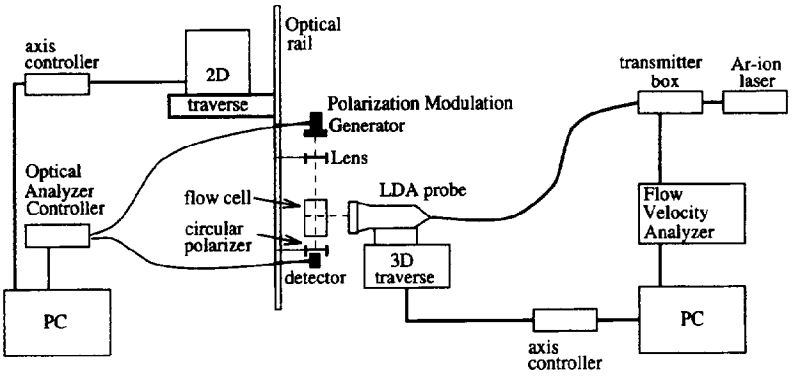

FIG. 1. Schematic drawing of the experiments: the view is along the (vertical) mean flow direction through the flow cell [with PMG: polarization modulation generator (laser, polarizer, rotating half-wave plate)]. Both FIB and LDA measurement systems, including the traverse tables, are controlled by a separate personal computer. Details of all equipment are given in Baaijens (1994).

$$\tau_{xy} = \frac{\Delta n}{2C} \sin 2\chi, \tag{7}$$

$$N_1 = \tau_{xx} - \tau_{yy} = \frac{\Delta n}{C} \cos 2\chi. \tag{8}$$

The system is capable of measuring birefringence as low as $\mathcal{O}(10^{-8})$, which is orders of magnitudes lower than for the (classical) field-wise "fringe-counting" method [$\Delta n = \mathcal{O}(10^{-4})$].

Control of the experiment and data acquisition are performed by the ROA software, that is implemented in the package LABView (National Instruments, LABView for Windows), with a personal computer (486DX-50 MHz, 8 Mb RAM) equipped with a data acquisition board (National Instruments, AT-MIO-16L9).

4. Measurement procedure

Figure 1 shows schematically the apparatus used in the experiments with the position of the two measurement systems relative to the flow cell. FIB and LDA measurements were performed simultaneously, but independently. Each system has its own computer controlled traverse. To be able to measure the centerline velocities near the cylinder, the LDA laser probe is positioned along the long side of the flow cell with the laser beams in the plane that is perpendicular to the axial (neutral) direction of the cylinder. This configuration also results in rapid data collection, since the light scattered in the whole solid angle of the laser probe is useful for detection of Doppler bursts.

During the LDA experiments the velocity was averaged from 100 acquired samples that satisfied the strongest validation criterion (+3 dB). Increasing the number of validated samples did not change the average velocity. A seeding of small particles (Merck Iriodine 111, coated rutile crystals, density $\rho \approx 2.5 \times 10^3$ kg/m^3, diameter particles $d_p \leq 15$ μm) was added in a concentration of approximately 0.01 g/ℓ to increase the data rate. The effective data rate (= number of validated samples per unit of time) was between 50 and 400 Hz. The seeding did not affect the birefringence measurements. The

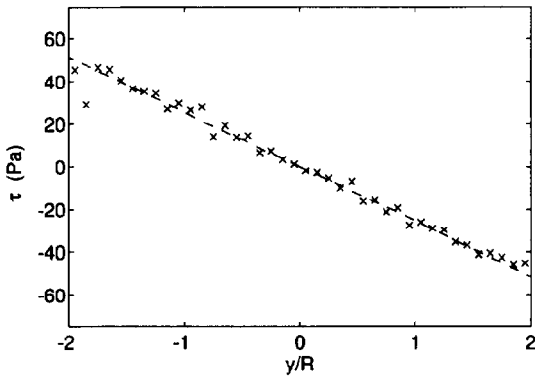

FIG. 2. Shear stress along a cross-sectional line in the fully developed flow region: (×) measured using literature value $C = 1.87\times10^{-9}$ Pa^{-1}, and (--) computed with a Carreau–Yasuda model at De = 2.32.

laser was operated at a power level of 70 mW, and the high voltage of the photomultiplier was between 1000 and 1096 V.

The laser beam of the birefringence measurements is collimated by a lens with focal length 400 mm, which gave a maximum beam radius of 0.35 mm at the exit and entrance windows of the flow cell (in later experiments, we have improved this to a maximum radius of 0.15 mm with another type of half-wave plate and a lens with $f = 800$ mm). From the measured birefringence parameters χ and Δn, the stresses were found using the stress optical rule. The stress optical coefficient as determined by Quinzani (1991) in a Couette flow cell was used: $C = 1.87\times10^{-9}$ Pa^{-1}. In a later experiment, we measured the stress optical coefficient ourselves in a Couette cell for simultaneous mechanical and optical (with ROA) measurements on the Rheometrics-RFS-II and found [Baaijens (1994)]: $C = 1.86\times10^{-9}$ Pa^{-1}, see Figs. 2 and 3.

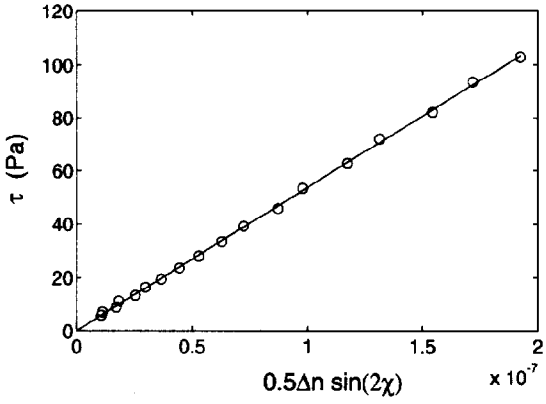

FIG. 3. Validation of linearity of stress optical rule in a self-constructed Couette cell on a Rheometrics-RFS-2 with simultaneous mechanical and optical measurements. The mechanical stress τ is plotted as function of the simultaneously measured optical signal $\Delta n/2 \sin 2\chi$; the stress optical coefficient follows from linear fit of data points: $C = 1.86\times10^{-9}$ Pa^{-1}.

TABLE I. Definition Y_i and ξ in Eq. (13), specifying several constitutive equations of the differential type. PTT = Phan-Thien–Tanner, **I**: unity tensor, ϵ, α: model parameters, tr(τ): trace of tensor τ.

Constitutive equation	Y_i	ξ
PTT-a	$e^{\epsilon_i \lambda_i / \eta_i \, \mathrm{tr}(\tau_i)}\mathbf{I}$	$0 < \xi < 2$
PTT-b	$[1+\epsilon_i \lambda_i / \eta_i \, \mathrm{tr}(\tau_i)]\mathbf{I}$	$0 < \xi < 2$
Giesekus	$(\mathbf{I}+\alpha_i \lambda_i / \eta_i \tau_i)$	0

The influence of parasitic birefringence effects of the viewing windows was minimized by the use of the Schott SF57 glass. In all cases, except at the lowest flow rate, it sufficed to subtract offset values for both R_1 and R_2. These offsets were measured during zero flow and were mean values of measurements taken in about 20 different spatial points spread over the domain. In case of the lowest flow rate, the small spatial variation in the offset values could not be neglected compared with the signal during flow. A special procedure was followed here: after measuring the signals R_1 and R_2 during flow and during zero flow, the latter values were subtracted point-wise from the first.

C. Mathematical problem definition and numerical methods

The flow field has been computed with finite element methods (FEMs) that are implemented in the package SEPRAN [Segal (1992)]. The mathematical problem to be solved is described by the equations for conservation of momentum:

$$\rho\left(\frac{\partial \mathbf{v}}{\partial t} + \mathbf{v}\cdot\nabla\mathbf{v}\right) - \nabla\cdot\boldsymbol{\sigma} = \mathbf{0}, \tag{9}$$

and conservation of mass:

$$\nabla\cdot\mathbf{v} = 0, \tag{10}$$

where $\mathbf{v}$ denotes the velocity field, ρ is the density, and $\boldsymbol{\sigma}$ the Cauchy stress tensor, defined as

$$\boldsymbol{\sigma} = -p\mathbf{I} + \boldsymbol{\tau}, \tag{11}$$

where $p(\mathbf{x},t)$ is the pressure field, $\mathbf{I}$ the unit tensor, and $\boldsymbol{\tau}$ the extra-stress tensor. The full equations of conservation of momentum were used, since the Reynolds number ranged between 0.029 and 0.174, and test runs had shown that neglecting the convective term $\mathbf{v}\cdot\nabla\mathbf{v}$ ("Stokes flow approximation") influenced the solution of the velocity field up to approximately 5%. The problem is defined completely when an appropriate constitutive equation is substituted for the extra-stress field $\boldsymbol{\tau}$.

For a generalized Newtonian fluid the relation

$$\boldsymbol{\tau} = 2\eta(II_D)\mathbf{D}, \tag{12}$$

holds, with $\mathbf{D}$, the rate-of-deformation tensor $2\mathbf{D} = \mathbf{L}+\mathbf{L}^T$, $\mathbf{L} = (\nabla\mathbf{v})^T$, and $\eta(II_D)$ a viscosity that depends on a generalized shear rate (via II_D: the second invariant of $\mathbf{D}$), for example the Carreau–Yasuda (CY) equation [Eq. (23)]. The viscoelastic models are defined by Eqs. (13)–(15) and Table I, together with the fitted parameters in Table II:

$$\hat{\tau}_i + \frac{1}{\lambda_i}\mathbf{Y}_i\cdot\boldsymbol{\tau}_i = \frac{2\eta_i}{\lambda_i}\mathbf{D} \quad i = 1,\ldots,N, \tag{13}$$

TABLE II. Parameter values for one-mode and four-mode (n: number of modes) nonlinear viscoelastic constitutive models at the reference temperature of 25 °C in the case of the 5% PIB/C14 solution [averaged time constant of four-mode fit $\bar{\lambda} = 4.31\times10^{-2}$ s, see Eq. (27)].

	Maxwell parameters		PTT		Giesekus	
n	η_i (Pa s)	λ_i (s)	ξ	ϵ	α	η_s (Pa s)
1	9.28×10^{-1}	2.90×10^{-2}	0.0	0.39	0.21	0.05
4	4.43×10^{-1}	4.30×10^{-3}	0.0	0.39	0.40	0.0
	4.40×10^{-1}	3.70×10^{-2}				
	9.20×10^{-2}	2.03×10^{-1}				
	1.70×10^{-3}	3.00×10^{0}				

with η_i, λ_i the parameters of a linear viscoelastic Maxwell model, $\mathbf{D}$ the rate of deformation tensor, i denoting a single mode, the tensor $\mathbf{Y}$ defined for some models in Table I and

$$\hat{\tau}_i = \frac{\partial \boldsymbol{\tau}_i}{\partial t} + \mathbf{u}\cdot\nabla\boldsymbol{\tau}_i - (\mathbf{L}-\xi\mathbf{D})\cdot\boldsymbol{\tau}_i - \boldsymbol{\tau}_i\cdot(\mathbf{L}-\xi\mathbf{D})^T, \tag{14}$$

the Gordon–Schowalter derivative with $\mathbf{u}$ the velocity field [$\mathbf{u} = \mathbf{u}(\mathbf{x},t)$, $\mathbf{x}$ the position, t the time), $\mathbf{L} = (\nabla\mathbf{u})^T$. Many other models can be found in for example Larson (1988). Often, a Newtonian ("solvent") term $2\eta_s\mathbf{D}$ is added to the viscoelastic extra-stress tensor, and the total extra-stress tensor for a model with N modes is then found from

$$\boldsymbol{\tau} = 2\eta_s\mathbf{D} + \sum_i^N \boldsymbol{\tau}_i. \tag{15}$$

1. Numerical method for generalized Newtonian models

Computations with the (generalized Newtonian) CY model have been made with the Galerkin method (with a Picard linearization of the nonlinear viscosity term), see Cuvelier *et al.* (1986). The velocity and pressure were discretized using the Crouzeix–Raviart $P_2^+ - P_1$ triangular element with extended quadratic basis functions for the velocity and a piecewise discontinuous linear basis function for the pressure. The pressure is eliminated with the penalty function method. Convergence of the iterative procedure was checked with

$$\frac{|u_k - u_{k-1}|_{\max}}{|u_k|_{\max}} < \epsilon_c, \tag{16}$$

$$\hat{R}_k < \epsilon_c, \tag{17}$$

with u_k the velocity after the kth iteration, $\hat{R}_k = |Au_{k-1}|_{\max}/|u_{k-1}|_{\max}$ the relative residual of the discretized system after iteration $(k-1)$ and $\epsilon_c = 1\times10^{-4}$.

2. Numerical method for viscoelastic models

The viscoelastic computations have been performed with the method for stationary two-dimensional flow of Hulsen (1988) [see also Hulsen (1990) and Hulsen and van der Zanden (1991)]. It is an iterative, decoupled method. The balance equations of mass and momentum are discretized with the standard Galerkin method (with the same element as in case of the generalized Newtonian method). The extra-stress tensor is computed from

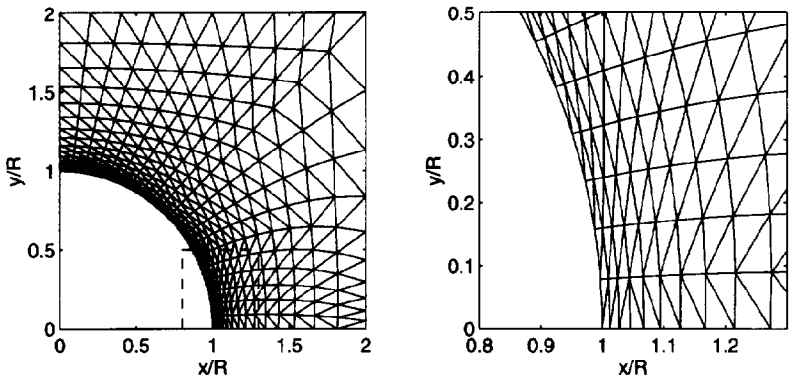

FIG. 4. Left: part of (symmetric) FEM mesh in the case of geometry with symmetrically confined cylinder. Right: enlarged region of FEM mesh (the same region as marked with the dashed box in the plot on the left).

the last computed velocity field by integration of the viscoelastic constitutive equation along the streamlines (these are computed from the velocity field via the stream function) with a fourth-order Runge Kutta scheme. A Picard iteration scheme is used to solve the resulting set of nonlinear equations. For details about the construction of the streamlines and the iterative procedure the reader is referred to Hulsen (1988) and Hulsen and van der Zanden (1991).

Convergence is tested after each iteration with

$$\frac{|u_{k+1}-u_k|_{\max}}{|u_{k+1}|_{\max}} < \epsilon_u, \tag{18}$$

$$\left(\frac{R^T R}{\hat{R}^T \hat{R}}\right)^{1/2} < \epsilon_r, \tag{19}$$

where u_k is the velocity after the kth iteration, and R is the residual value of system of equations for the "free" degrees of freedom (thus without the essential boundary conditions) for the discretized momentum equation and ϵ_u, ϵ_r^2 the convergence criteria (both usually 1×10^{-3}).

Part of the FEM mesh used in all computations is plotted in Fig. 4; the complete mesh has 1900 elements and 3981 nodal points. The resulting problem has 7962 degrees of freedom (velocities only) in case of both the viscoelastic constitutive equation and the generalized Newtonian model. Mesh refinement in both x and y direction with a factor 1.5 did not influence the solution significantly.

3. Definition of boundary conditions

Denote the velocity vector with $\mathbf{u}$, the outward normal on a boundary with $\mathbf{n}$, the tangential vector on the boundary with $\mathbf{t}$, and the Cauchy stress tensor with $\boldsymbol{\sigma}$. The boundary conditions are then defined by the symmetry condition

$$\mathbf{u}\cdot\mathbf{n} = 0, \tag{20}$$

$$\mathbf{t}\cdot(\boldsymbol{\sigma}\cdot\mathbf{n}) = 0 \tag{21}$$

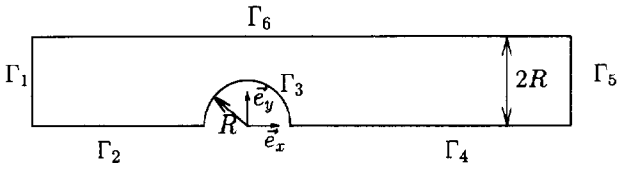

FIG. 5. Geometry with boundaries Γ_1–Γ_6 (boundary conditions: see text); x positions of boundaries Γ_1 and Γ_5 are not plotted on scale (Γ_1 at $x = -5R$ and Γ_5 at $x = 15R$).

along the centerline boundaries Γ_2 and Γ_4 (see Fig. 5), and the no-slip condition

$$\mathbf{u} = \mathbf{0} \tag{22}$$

on the boundaries Γ_3 and Γ_6. At the entrance (Γ_1) and exit (Γ_5) boundaries, fully developed flow conditions were assumed in case of the viscoelastic computations, which were calculated numerically for the model used. In case of the generalized Newtonian model, it was convenient to prescribe a Newtonian velocity profile at entrance and exit boundaries. It was proven that it did not affect the solution in the region of interest.

III. RESULTS

A. Rheological characterization and parameter determination in simple shear flow

Experiments in both steady and small amplitude oscillatory simple shear flow are used to fit parameters of nonlinear viscoelastic constitutive equations. Predictions in planar elongation are analyzed for various fits of constitutive equations.

Master curves for $\eta(\dot{\gamma})$, $N_1(\dot{\gamma})$, $\eta'(\omega)$, and $\eta''(\omega)$ at a reference temperature of 25 °C were created after time–temperature superposition [Ferry (1980)].

The four plots in Fig. 6 show that the shifting procedure results in smooth master curves for both η and N_1 in steady shear, and η' and η'' in small amplitude oscillatory shear. The master curve for N_1 is shown for the range of shear rates where the data are not scattered too much. At shear rates lower than plotted the scatter was unacceptably large.

The viscosity function in steady simple shear flow was fitted with the (generalized Newtonian) Carreau–Yasuda (CY) model:

$$\eta = \eta_{CY}[1+(\lambda_{CY}\sqrt{II_D})^a]^{(n-1)/a}, \tag{23}$$

which gave as fitted values for $\{\eta_{CY},\lambda_{CY},a,n\}$: (0.96 Pa s, 0.02 s, 1, 0.45) (this fit is plotted in Fig. 7).

As viscoelastic models, the Phan-Thien–Tanner-b (PTT-b) equation and the Giesekus equation have been fitted on the data in Fig. 6. Armstrong *et al.* (1992), who compared six models, showed that these two models describe stresses of this fluid along the centerline in a four to one contraction flow most adequately.

The parameters of the viscoelastic constitutive equations were fitted using the following procedure. First, the Maxwell parameters $\{\eta_i,\lambda_i\}$ were determined by fitting the linear viscoelastic Maxwell model to the complex viscosity with a Levenbergh–Marquardt method [see Zoetelief (1992)]. The components of the complex viscosity for a multimode Maxwell model:

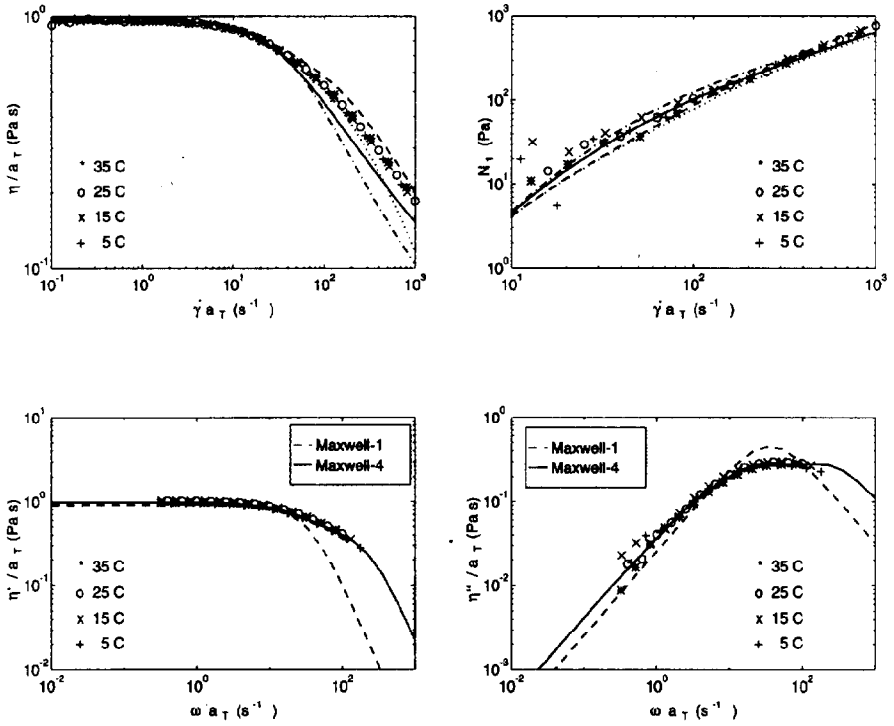

FIG. 6. Master curves at T_{ref} = 25 °C in simple shear flow for the 5% PIB/C14 solution. Top: steady shear viscosity $\eta(\dot{\gamma})$ and first normal stress difference $N_1(\dot{\gamma})$ together with four fitted constitutive equations [(–) denotes the PTT model with one mode, (– –) denotes the PTT model with four modes, (–·–) denotes the Giesekus model with one mode, (···) denotes the Giesekus model with four modes]. Bottom: complex viscosity with fitted Maxwell models ("Maxwell-1:" Maxwell model with one mode).

$$\eta' = \sum_{i}^{N} \frac{\eta_i}{1+\omega^2\lambda_i^2}, \tag{24}$$

$$\eta'' = \sum_{i}^{N} \frac{\eta_i\lambda_i\omega^2}{1+\omega^2\lambda_i^2}, \tag{25}$$

where i represents the number of a mode, and N is the number of modes. A one-mode and a four-mode model were fitted. Both results are plotted in Fig. 6, and the parameter values are tabulated in Table II.

Second, the nonlinearity parameters in the nonlinear viscoelastic PTT and Giesekus equations were determined by minimizing

$$q = \sum_{j} \left[\left(\frac{N_{1,j} - N_{1,j}^{\exp}}{N_{1,j}^{\exp}} \right)^2 + \left(\frac{\eta_j - \eta_j^{\exp}}{\eta_j^{\exp}} \right)^2 \right], \tag{26}$$

where the index j denotes a shear rate value, $N_{1,j}$ denotes the first normal stress difference, η_j the shear viscosity, and the superscript exp denotes the measured value. The residue q was minimized with respect to the nonlinearity parameters by a trial and error

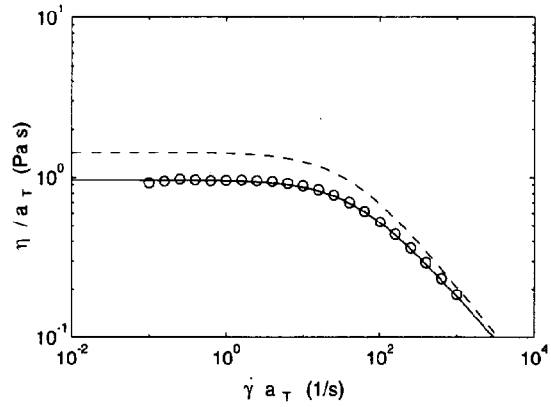

FIG. 7. Comparison of our measured steady shear viscosity and Carreau–Yasuda (CY) fit with the CY fit of Quinzani (1991) for 5% PIB/C14 [open symbols denote the measured data for the current fluid, (–) denotes the fit on the data of the current fluid, (– –) denotes the fit of Quinzani].

variation of these parameters and evaluation of q. Stresses were calculated by solving numerically the nonlinear system of equations for the constitutive equations in steady simple shear flow with a Gauss–Newton method as implemented in Matlab (The MathWorks Inc., function "fsolve"). In the case of the one-mode fit, the solvent contribution to the extra-stress tensor ($2\eta_s\mathbf{D}$) was used to adjust the zero-shear-rate viscosity level (the viscosity of tetradecane is 0.002 Pa s). In the case of the four-mode fit, the "solvent" viscosity was neglected ($\eta_s = 0$). All parameters of the nonlinear viscoelastic equations used are tabulated in Table II. For a multimode model the viscosity average value for the time constant, $\bar{\lambda}$, is defined by

$$\bar{\lambda} = \sum_i \eta_i \lambda_i \Big/ \sum_i \eta_i. \tag{27}$$

The four-mode PTT model fits the measured viscosity best of all four fits that have been evaluated, see Fig. 6, where the results for the two nonlinear viscoelastic models are shown. The single-mode models fit the steady shear viscosity equally well as the four-mode models for shear rates up to 40 s^{-1}, i.e., until shear thinning has just started. For higher shear rates the single-mode Giesekus model predicts a too strong shear thinning and its prediction of the viscosity is worst of all four fits. The two four-mode fits are both more accurate than the one-mode PTT model for shear rates between 80 and 500 s^{-1}. At higher shear rates the four-mode Giesekus model is again too shear thinning. Although the same holds for the one-mode PTT model, the effect is less serious and its prediction of the viscosity still agrees fairly well with the measured data.

Although differences between the fits are small, the normal stress difference N_1 is fitted best by the one-mode PTT model for shear rates below 200 s^{-1}, while for higher shear rates the prediction of the four-mode PTT model is best. The differences between results for the Giesekus model are larger.

Quinzani *et al.* (1990) have characterized the rheology of this solution in simple shear flow, and our results can be compared with those. In Fig. 7 our steady shear viscosity and the fits of the CY model of Quinzani ($n = 0.4$, $\eta_{CY} = 1.424$ Pa s, $a = 1$, $\lambda_{CY} = 0.024$ s) are plotted together. It clearly reveals differences between the fluids. The zero shear viscosity at 25 °C in our measurements is 0.96 Pa s, while Quinzani's result is 1.424 Pa s.

Our data proved to be reproducible with each new batch of fluid made, and the large difference between our zero shear viscosity and Quinzani's is probably caused by differences in the molecular weight distributions of the PIB batch used.

In the present study, the parameter ξ in the PTT equation has not been used, since it did not improve any of the fits. Moreover, a nonzero ξ parameter is known to cause oscillations in stresses during start-up of steady shear. We also aimed to fit the data with as few parameters as possible. Therefore the four-mode equations were fitted with a single value for ϵ or α for all modes.

1. Start-up of simple shear flow

Shear stresses have been measured during start-up of simple shear flow, for four values of the final shear rate $\dot{\gamma}_0$: 10, 30, 60, 100 (1/s). (Unfortunately, no reliable transient measurement of normal stress was possible, due to too great an oscillation in the normal force that depended on the rotation frequency of the plate.) The transient viscosity function η^+ is defined as

$$\eta^+ = \frac{\tau}{\dot{\gamma}_0}. \tag{28}$$

The measured data have been compared with model predictions with parameters from Table II. Stresses were calculated with a fourth- and fifth-order Runge–Kutta integration, with automatic step size control (as implemented in Matlab, The MathWorks Inc.). To avoid the singularity in the stresses at $t = 0$ s, a ramp of 0.02 s has been used in the shear rate history during the calculations. The results are shown in Fig. 8 (single- and four-mode PTT model and single- and four-modes Giesekus model).

Differences between computations and measurements are mainly due to differences in the steady state value for η. This steady-state value is predicted accurately by all four models at shear rates of 10 and 30 s^{-1}. At higher shear rates (60, 100 s^{-1}), however, both four-mode models proved to be more accurate than the single-mode models. It also appears that for the two highest shear rates all models predict an overshoot, that is largest in case of the Giesekus models. A small overshoot is also present in the measured data and the PTT models have an overshoot that is closer to the measured data than do the Giesekus models.

2. Predictions in planar elongational flow

Model predictions in steady planar elongation are compared for the different models in Fig. 9. All fitted viscoelastic models show modest elongation thickening behavior, i.e., an increase in elongational viscosity with increasing elongation rate. The effect is controlled by the value of the nonlinearity parameters ϵ and α in the PTT and Giesekus model, respectively. The smaller these values, the stronger the elongation thickening (in the limit $\epsilon \to 0$ or $\alpha \to 0$ the models change into the UCM model that has infinite extensional stresses above a certain extension rate). The single-mode Giesekus model possesses a higher elongational viscosity than the other models: this is due to the relatively low value of the parameter α, see Table II.

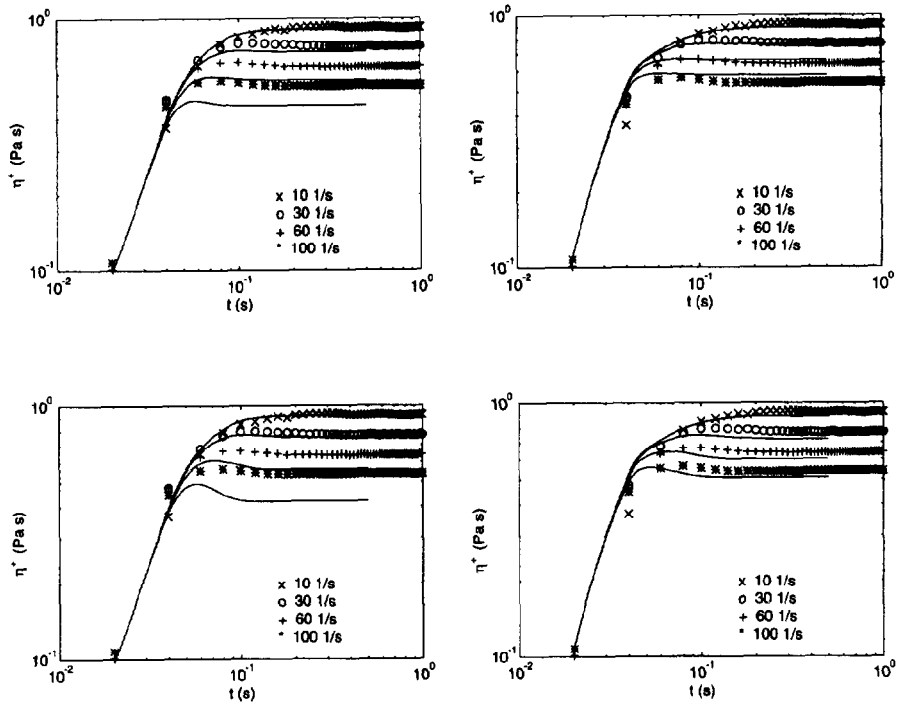

FIG. 8. Viscosity η^+ during start-up of steady simple shear flow at $T = 25$ °C for the 5% PIB/C14 solution. Top: single-mode (left) and four-mode (right) PTT model. Bottom: one-mode (left) and four-mode (right) Giesekus equation.

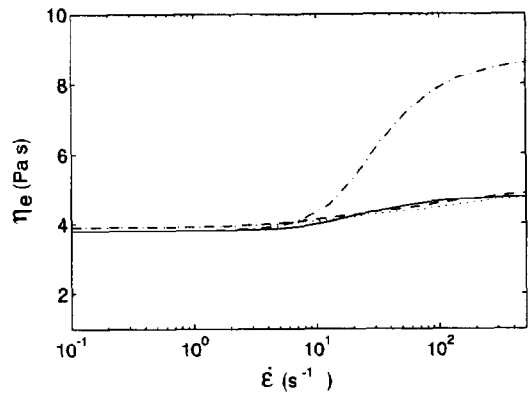

FIG. 9. Predictions in planar elongation of viscoelastic constitutive equations with parameter values fitted in simple shear flow for the 5% PIB/C14 solution. [(–) denotes the PTT model with one mode, (– –) denotes the PTT model with four modes, (–·–) denotes the Giesekus model with one mode, (···) denotes the Giesekus model with four modes].

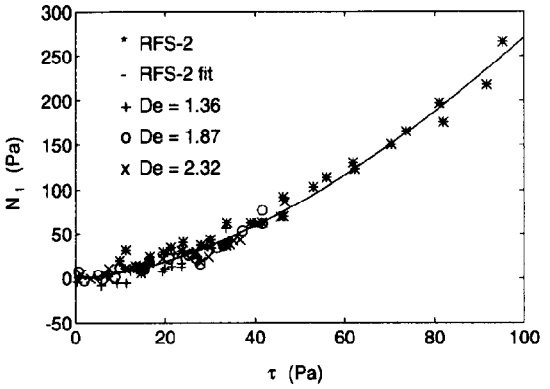

FIG. 10. Normal stress as function of shear stress for 5% PIB/C14. Data consist of measurements in simple shear (RFS-2) and their fit (RFS-2 fit, with $N_1 = a\tau^b$, (see text) together with stresses measured with FIB along a cross section in the fully developed flow region in the planar flow cell at three De numbers.

B. Flow past a confined cylinder

1. Demonstration of LDA and FIB techniques in fully developed slit flow

The accuracy of the LDA measurements is demonstrated by the excellent agreement between calculated velocities and measured velocities in the fully developed flow at $x/R = -5.0$ as shown in Figs. 12–14), in combination with a maximum noise level of 3% in the measured velocities.

The excellent agreement between computations and measured stresses in the fully developed flow region at $x/R = -5.0$ in Fig. 2 and in Figs. 12–14 proves the accuracy of the stress measurements and of the value for the stress optical coefficient ($C = 1.87\times10^{-9}$ Pa^{-1}).

To demonstrate further the accuracy of the optical stress measurements, the stresses measured in simple shear with the Rheometrics-RFS-2 (cone and plate geometry) are plotted together with the stresses as measured at three different flow rates in fully developed flow that is also a simple shear flow. Figure 10 shows N_1 as a function of τ. The measured curve of $N_1(\tau)$ on the RFS-2 has been fitted with the relation $N_1 = a\tau^b$ with $a = 0.13$ Pa$^{(1-b)}$ and $b = 1.66$. A good agreement is found, and the scatter in the optically measured data is of the same magnitude as in the mechanically measured data [in later experiments we improved the optical part of our ROA system such that the radius of the laser beam was a factor of two smaller and the optical data have even significant less scatter than the mechanical data, see Figure 4.23 in Baaijens (1994)].

2. Symmetrically confined cylinder

Experiments were carried out at an ambient temperature of 24±0.5 °C. Stresses and velocities were measured along five cross-sectional lines: $x/R = -5$, -2.0, -1.5, 1.5, and 2.0, and along the centerline: $y/R = 0$ [(x,y) coordinates are defined in Fig. 5].

Velocities are made dimensionless with the mean velocity U, and stresses with

$$\tau_0 = 3\eta_0 U/R, \tag{29}$$

where η_0 is the zero shear viscosity. The factor 3 in this definition of τ_0 is arbitrary and is added only to obtain a scaling that fitted nicely in the plots of Figs. 12–14. Table III

TABLE III. Mean velocity U, typical shear rate U/R, scaling stress τ_0, and dimensionless numbers De, Re, for the cases studied in the geometry with the symmetrically confined cylinder [definitions of τ_0, De, and Re in Eqs. (29)–(31), respectively].

U (m/s)	U/R (s^{-1})	τ_0 (Pa)	De	Re
0.0115	5.750	16.865	0.248	0.019
0.0424	21.200	62.179	0.931	0.069
0.0633	31.650	92.828	1.364	0.102
0.0868	43.400	127.291	1.871	0.140
0.1074	53.700	157.500	2.315	0.174

shows the values for the nondimensionalizing parameters U and τ_0, together with the Deborah number De and Reynolds number Re. The Deborah number is defined by

$$\mathrm{De} = \lambda_f \dot{\gamma}_c, \tag{30}$$

where λ_f is a characteristic relaxation time of the fluid [the average Maxwell time as defined in Eq. (27)] and $\dot{\gamma}_c$ is a characteristic shear rate (= inverse process time).

We define the Reynolds number Re as

$$\mathrm{Re} = Ud\rho/\eta_0, \tag{31}$$

with U a characteristic velocity of the flow, d a characteristic length of the geometry, ρ the density of the liquid, and η_0 the zero shear viscosity. Here we used for U the mean velocity and for d the cylinder radius.

The results are presented in this article only for three of the five cases in Table III: De = 0.25, 0.93, and 2.32. Results for the two other intermediate cases (De = 1.36, 1.87) can be found in Baaijens (1994). In all cases we observed stable flows. Samples of the fluid were regularly taken to monitor their rheology by steady and dynamic tests on the Rheometrics-RFS-2. No changes were found. Model parameters are used as fitted at a reference temperature of 25 °C.

The four-mode PTT model was used as viscoelastic constitutive equation, since it was found above that this model fitted data in simple shear flow well. The single-mode PTT model was used to demonstrate the differences between a single-mode and a multimode model in the complex flow. The computations with these viscoelastic models were made by step-wise increasing the flow rate: first, at the lowest flow rate the solution was obtained with the iterative procedure and the result was used as the starting solution for the computation at a higher flow rate. The number of iterations for each flow rate is given in Table IV. Note that the use of the four-mode model decreased the number of iterations.

LDA measurements along the third, "neutral" direction at two positions (at $x/R = -5$ and $x/R = 1.5$) show the assumption of a nominally two-dimensional flow field is good, see Fig. 11.

The results for the velocity and stress field, numerical as well as experimental, are presented along several cross-sectional lines in Figs. 12–14 and along the center line in Fig. 15. In Figs. 12–14, dimensionless velocities are plotted in the top graph, dimensionless first normal stress differences in the middle graph, and dimensionless shear stresses in the bottom graph. The base line of all cross-sectional profiles is depicted with a dotted vertical line. Subsequent curves from left to right correspond with subsequent dotted base lines. The "x/R" ordinate of the kth cross section ($k = 1,2,\ldots,M$; the number of cross sections M varies with the plots) is denoted with X_k. Actual values for velocity or stress can be obtained by multiplying the plotted dimensionless value (that is found by reading

TABLE IV. Mean velocity U and number of iterations n_{iter} for the computations with the one- and four-mode PTT equations, in the case of the geometry with the symmetrically confined cylinder. The solution at each (except the lowest) flow rate was obtained by using the result of the previous (lower) flow rate.

U (m/s)	n_{iter} PTT-1	n_{iter} PTT-4
0.0424	29	13
0.0633	26	12
0.0700	22	6
0.0800	25	8
0.0868	22	6
0.1074	33	11
Σn_{iter}	157	56

of its horizontal ordinate on the "x/R" axis minus the ordinate X_k of the corresponding base line) with the number used for the scaling (U or τ_0, see Table III).

3. Axial velocity field

The graphs on top of Figs. 12–14 present the results of the computations and experiments for the axial velocity field along several cross sections, while the middle and bottom graphs show the results for the first normal stress differences and shear stress, respectively.

A small asymmetry is observed in the measured velocity profiles. This is explained by an eccentricity in the placement of the cylinder between the walls. In Baaijens (1994) it is shown, that in case of an eccentricity as little as $0.05R$(= 0.1 mm), the four-mode PTT model predicts a more asymmetric axial velocity field than the measurements. Interestingly, these predictions also showed that the stress profiles are less sensitive to this eccentricity than is the velocity field. It is estimated that a negligible degree of asymme-

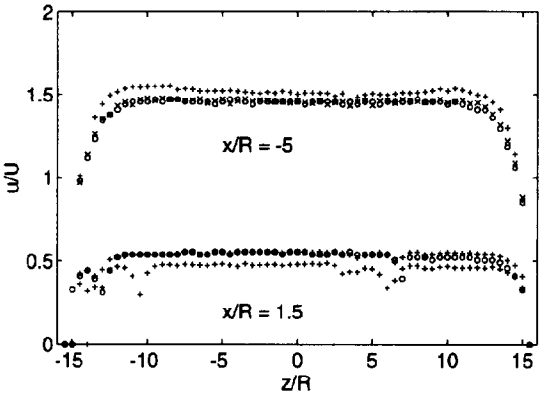

FIG. 11. Measurement of the axial velocity along the neutral (z) direction at two positions ($x/R = -5.0,1.5$) and three flow rates [(+): U = 0.0118 (m/s), (×): U = 0.0424 (m/s), and (○): U = 0.0633 (m/s)] that shows the flow is nominally two-dimensional.

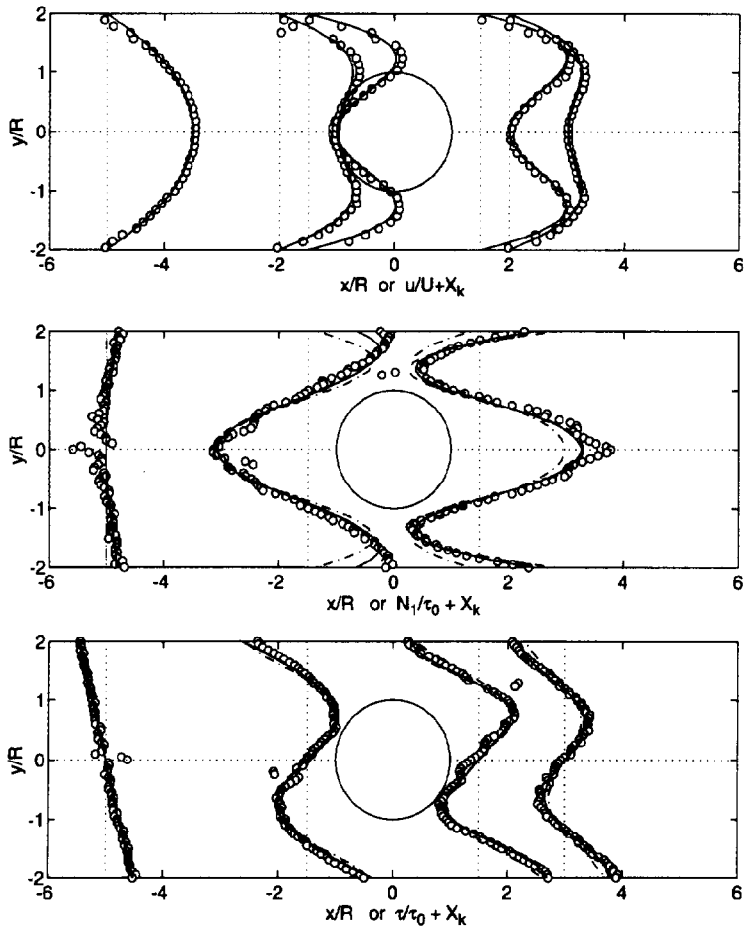

FIG. 12. Measured (○) and computed [(–) four-mode PTT model, (– –) one-mode PTT model, (–·–) CY model] results for the planar flow of the 5% PIB/C14 solution at De = 0.25 past a cylinder confined symmetrically between two parallel plates. Velocities are made dimensionless with the mean velocity U and stresses with τ_0. X_k denotes the x/R coordinate of the base line corresponding with each separate curve (see text).

try in the experimental flow field (with the distance between the walls of $4R$ and a cylinder with radius R) can only be obtained in a flow cell with an eccentricity below $0.01R$.

At all Deborah numbers excellent point-wise agreement is found between the measured axial velocities and those computed with the CY model. The results for the single- and four-mode PTT model agree excellently with measured data at the two lowest Deborah numbers (De = 0.25, 0.93). The good agreement between computed and measured axial velocities at De = 0.25 for all models (Fig. 12) was expected, since for De $\rightarrow$ 0, the flow behavior becomes Newtonian. At De = 2.32, the agreement is good for the four-mode model and fairly good for the single-mode model.

The most pronounced differences between the computed results for both fits of the PTT model and the measured velocities exist at De = 2.32 along the downstream cen-

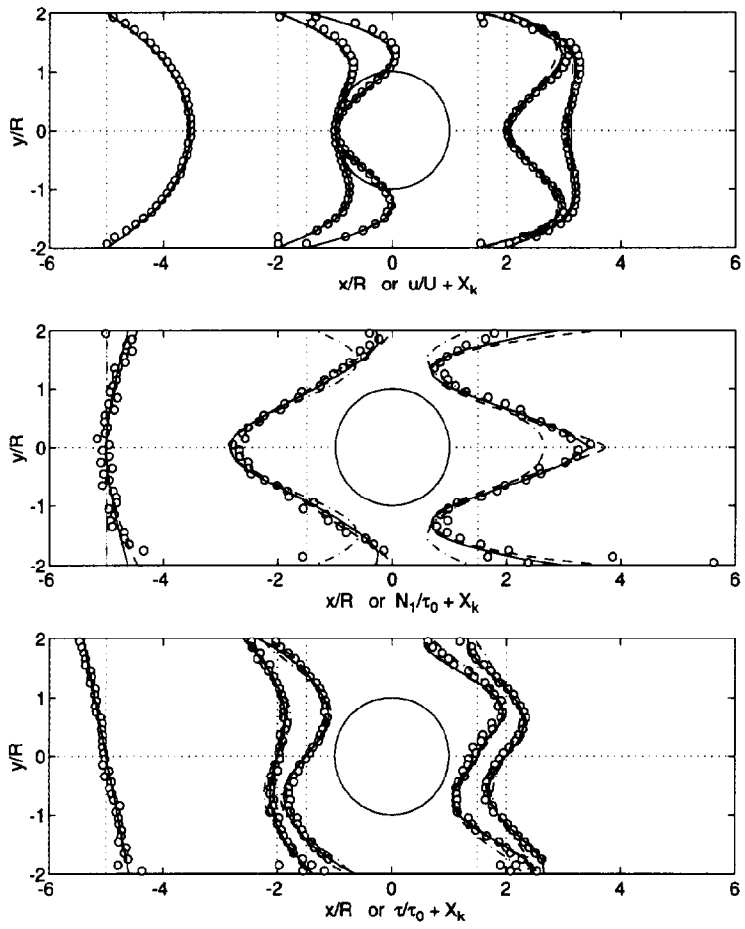

FIG. 13. As in Fig. 12, now with De = 0.93.

terline ($x > 0$, $y = 0$). Immediately downstream of the cylinder, the calculated axial velocities for the PTT models show an overshoot compared with the measurements. The effect is strongest for the single-mode PTT model: a relatively large overshoot in the velocity profile is observed. The overshoot is completely absent in the measured velocities and in the results for the CY model. In the case of the axial velocities, the results for the four-mode PTT model show a remarkable improvement compared with those for the single-mode fit, but some quantitative differences with the measured velocities remain.

4. Stress field

Good agreement is found between computed and measured stresses at all flow rates with both PTT fits, and sometimes the agreement is excellent (Figs. 12–15). In the plots along cross lines, the profiles of N_1 at $x/R = 2.0, -2.0$ are left out to improve the clarity of the plots.

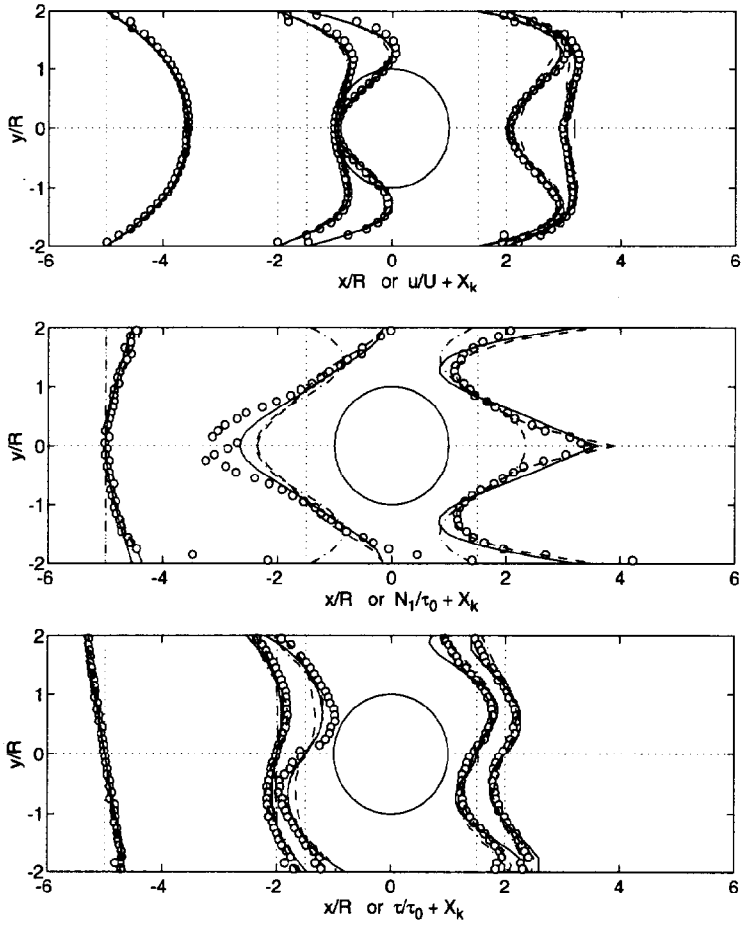

FIG. 14. As in Fig. 12, now with De = 2.32.

At the lowest Deborah number (De = 0.25) the predictions of the shear stresses for both PTT models and the generalized Newtonian model agree excellently with measured data (Fig. 12). The PTT models also predict excellently the normal stress differences. The results obtained with these two fits cannot be distinguished at any position at this low Deborah number. The only difference between the simulations with the PTT models and the measurements is that they predict too low a maximum in the cross-sectional normal stress profile at $x/R = 1.5$. Except near the confining walls, the CY model predicts the normal stress difference along the cross section $x/R = -1.5$ excellently, thus apparently elasticity is not important here. In the fully developed flow region and near the confining walls the CY model clearly fails to predict the measured normal stress differences, of course, since it cannot predict normal stresses in shear flow. This effect is independent of the Deborah number and is not discussed in case of the other two Deborah numbers below. Along the cross section $x/R = 1.5$, the CY model predicts the normal stress difference well; its maximum value near the center line is lower compared with the PTT

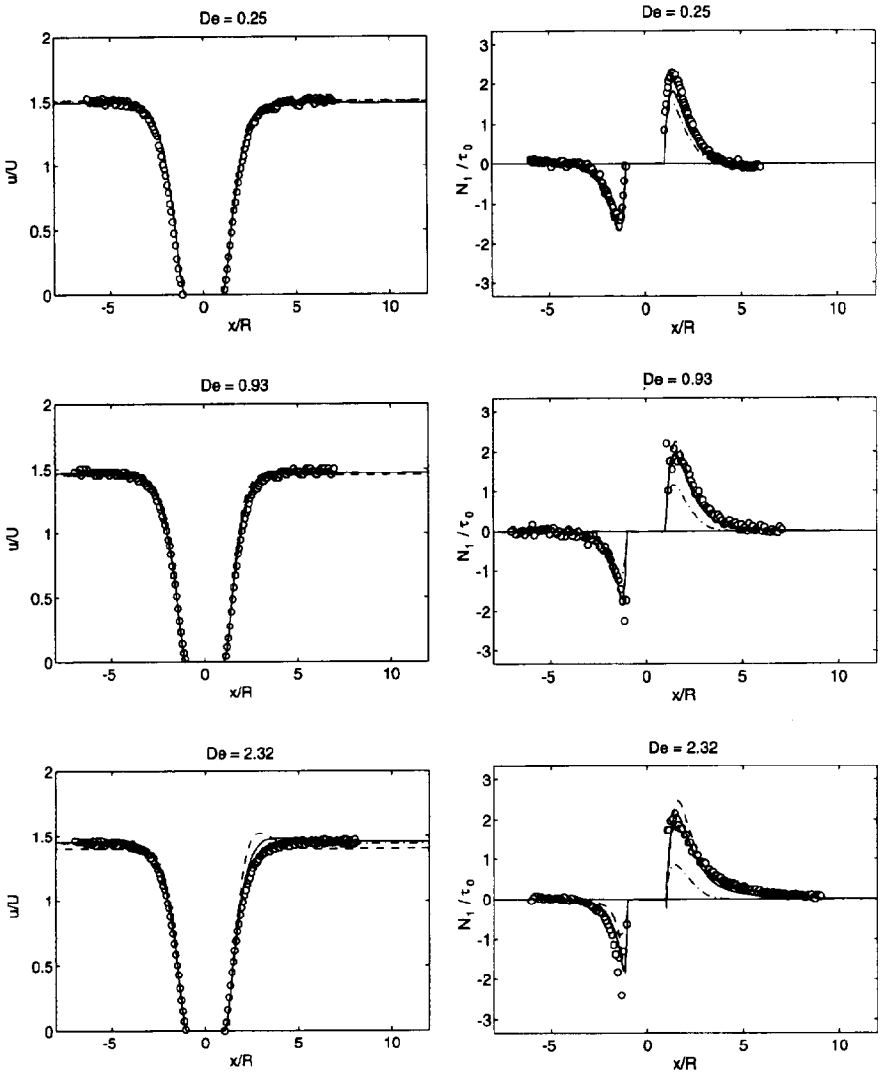

FIG. 15. Measured (O) and computed [(–) four-mode PTT model, (– –) one-mode PTT, (–·–) CY] velocity (left) and first normal stress difference (right) along the centerline for the flow of the 5% PIB/C14 solution past a symmetrically confined cylinder, for De = 0.25, 0.93, 2.32. Velocities are made dimensionless with mean velocity U, stresses with τ_0 (see text).

models as is also clear from Fig. 15. Thus a small influence of the elastic response of the fluid is already present at this low flow rate.

At De = 0.93, excellent agreement is found between computed and measured shear and normal stresses for both PTT models along all cross sections (Fig. 13). Differences between these two models are negligible except for the maximum value of N_1 at $x/R = 1.5$ and near the side walls. At that position the single-mode PTT model has a higher maximum than the four-mode model. Upstream of the cylinder, the CY model predicts

the normal stress difference along $x/R = -1.5$ excellently, except near the confining walls. The CY model underpredicts the normal stress differences along the centerline downstream of the cylinder (see also Fig. 15), thus now the stress field is clearly influenced by the elastic response of the fluid to the history of the deformation.

At De = 2.32, more pronounced differences are found. In the experiments, the presence of the cylinder is manifest further upstream of the cylinder than in the computations: the minimum normal stress difference along cross section $x/R = -1.5$ is lower for the measured data than for both PTT models and the CY equation. Downstream of the cylinder, the four-mode PTT model predicts the normal stress differences excellently, except the minima of the cross-sectional profile along $x/R = 1.5$. Good agreement is also found for the single-mode model, it has, however, a maximum in the normal stress profile along the centerline that is too high. Again, the CY model predicts too low values for the normal stress difference near the downstream centerline. All three models predict the shear stress profiles well downstream of the cylinder, but upstream of the cylinder the agreement is only reasonable. Along $x/R = -1.5$, the prediction with the single-mode PTT fit differs mostly from the measured shear stress. The results for the four-mode PTT model and the CY model coincide at this site and agree fairly well with the measured shear stress profile. Along $x/R = -2.0$, both PTT models predict the measured shear stress profile excellently, while now the shear stress profile for the CY model is not in accordance with measured data except near the walls.

The measured velocities along the center line have been fitted with polynomials to calculate the elongational velocity gradient (elongation rate) along this line. The results are plotted in Fig. 16. It appears that the elongation rate is minimal $\approx -65\ s^{-1}$ upstream of the cylinder, and maximal $\approx 70\ s^{-1}$ downstream of the cylinder at the highest flow rate. This magnitude is an order higher than in the study of Armstrong *et al.* (1992), where the maximum elongation rate was $\approx 10\ s^{-1}$. Hencky strains ϵ_H were computed with

$$\epsilon_H = \int_0^{t_e} \dot{\epsilon}(t')dt' = \int_R^{5R} \frac{dv(x)}{dx}\frac{1}{v(x)}dx, \tag{32}$$

using the polynomial fits for $dv(x)/dx$ and $v(x)$, as $\epsilon_H = 0.37 \pm 0.03$ for the five flow rates. Thus the strain along the centerline is nearly invariant with flow rate and relatively low {compare with $\epsilon_H = 3$–7 for extensional rheometers [Macosko (1994)]}.

5. Comparison with results of Baaijens et al. (1994)

The above results for the stresses are not in accordance with those presented in our earlier study Baaijens *et al.* (1994) (see also *Note added in proof* in Baaijens *et al.* (1994)). We are now convinced that the discrepancy between the results in Baaijens *et al.* (1994) and the present results can only be explained by a change in the rheological behavior during the former experiments.

In Baaijens *et al.* (1994), we discussed two possible nonstatistical errors that might have affected the stress measurements: (i) influence of the subtraction procedure to account for the parasitic birefringence in the glass windows (due to the clamping of the windows in the flow cell and to the pressure build-up in the fluid during flow), (ii) failure of the stress optical rule in the elongational flow past the cylinder.

Failure of the stress optical rule is rather unlikely, in view of the results of Quinzani (1991) in the four to one contraction. Our results in this article confirm this statement.

We showed in Baaijens *et al.* (1994) that the effect of the fluid pressure on the window strain can be neglected. The subtraction procedure itself is legitimate in the limit of small

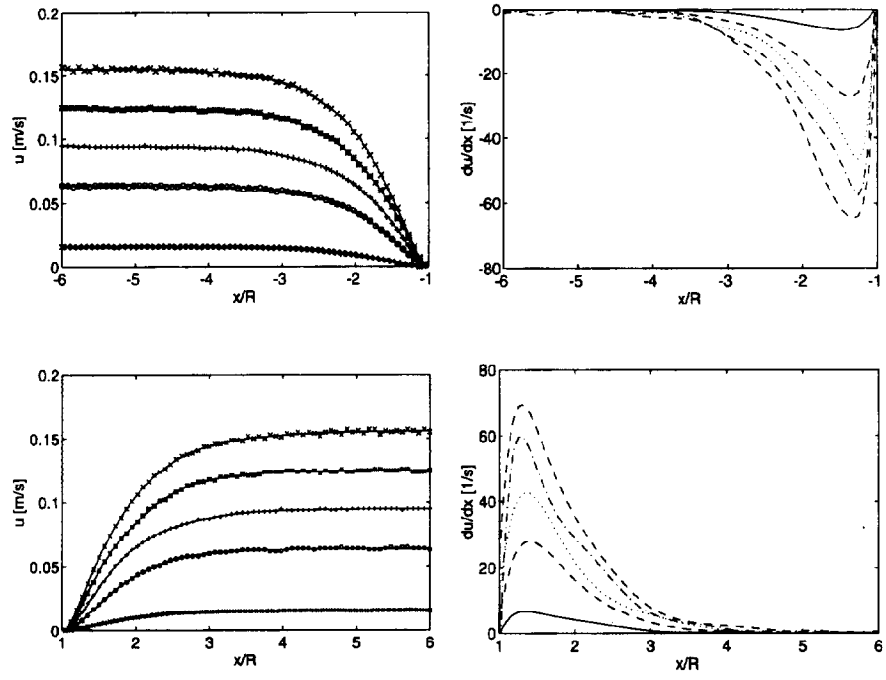

FIG. 16. Polynomial fit of measured velocities along centerline past the symmetrically confined cylinder (left) and the derivative of fitted polynomial (right) at the five Deborah numbers investigated (see Table III). Top row: upstream of cylinder, bottom row: downstream of cylinder. De = 0.25, 0.93, 1.36, 1.87, 2.32.

birefringence [see also Galante and Fratini (1993)]. The SF-57 glass used in the present study, instead of BK-7 glass in Baaijens *et al.* (1994), simplified the subtraction procedure, since a single off-set value was sufficient to shift the measurements at all spatial positions. Only at the lowest flow rate (De = 0.25) we still needed to measure the birefringence during zero flow at all positions. The result after point-wise subtraction is excellent: smooth symmetric stress profiles and excellent agreement with computational results for all models.

To investigate the effect of the subtraction procedure further, we replaced in our present flow loop the new flow cell by the one we used in Baaijens *et al.* (1994), thus with the BK-7 glass. At De = 0.25, using the point-wise subtraction procedure, we now found excellent agreement between the results with this flow cell and those obtained with the new cell [Schoonen (1994)].

It is remarkable that in all these latest experiments we were able to obtain smooth and symmetric stress profiles at the low Deborah number of 0.25 even in the developed flow region. In the previous study Baaijens *et al.* (1994) we only measured distorted, noisy profiles at this site. This despite the fact that in the older flow cell the light path through the flow cell was even a factor of 2 longer, which would benefit the accuracy of the measurement of birefringence (which is proportional with the length of the light path). It appears, that our present ROA system has a better resolution for the stresses than the system we used in Baaijens *et al.* (1994). Also, our present system is in this respect

superior to the two-color system of Quinzani (1991), who also was not able to measure stresses in fully developed flow at De = 0.25 for the similar model fluid.

From a methodological point of view, it is important to be able to measure stresses in fully developed flow to be able to demonstrate the measurement technique and to quantify its accuracy, since then the shear stress is described by a generalized Newtonian model. Several facts were in favor of the adequacy of the stress measurements in Baaijens *et al.* (1994): (i) the centerline stresses upstream of the cylinder did agree well with the computations, and the differences between computed and measured stresses existed downstream of the cylinder in the region where the fluid relaxes from the mixed shear and elongational flow; (ii) only after the point-wise subtraction procedure was the symmetry of the cross-sectional stress profiles excellent; (iii) the results reproduced well.

All together, we measured fluid properties in the former experiments and not just an artifact caused by the experimental apparatus. Unfortunately, up to now we have not been able to reproduce those results afterwards with a new fluid and despite many systematic attempts, we could not yet identify the reason that has caused the different behavior. In any event, the measured stresses as reported in Baaijens *et al.* (1994) should be considered as not representative for the present 5% PIB/C14 solution.

C. Asymmetrically confined cylinder

As a second step, the influence of viscoelasticity on the flow in a channel with an asymmetrically confined cylinder was investigated. We expected that this asymmetrical flow would be more sensitive for viscoelastic stresses such that also the velocity field should be influenced (see also Sec. I B). Since in the previous section the four-mode PTT model proved to be superior to the one-mode fit, here only the four-mode PTT fit will be used in the viscoelastic computations.

The cylinder was moved 1 mm towards one of the walls relative to the symmetrical situation, which resulted in a narrower gap between the wall and the cylinder of 1 mm at that side of the cylinder and a wider gap of 3 mm on the other side. Keeping $x/R = y/R = 0$ in the center of the cylinder, the wall that is closest to the cylinder is at $y/R = 1.5$, and the other wall at $y/R = -2.5$.

1. Experimental and numerical aspects

Measurements of the axial velocities and the stresses have been performed along cross-sectional lines at $x/R = -5.0, \pm 2.5, \pm 2.0, \pm 1.5, 0.0$ and along axial lines at $y/R = 0, -1.5$. The flow rate was set such that the mean velocity was 0.0868 m/s and thus De = 1.87. The stress measurements were performed with a lens with a focal length $f = 200$ mm, which resulted in a maximum beam radius at the exit and entrance planes of the flow cell of ≈ 0.25 mm.

The same numerical method was used as in the previous section. Parts of the mesh are shown in Figs. 17 and 18: the total mesh has 5364 elements and 11014 nodal points.

Both the generalized Newtonian CY model and the four-mode PTT equation were used, with parameter values as in Sec. II. Convergence was obtained with the convergence criteria as in Sec. II C. In case of the PTT equation, computations were performed by increasing the flow rate stepwise using each intermediate result as a starting value for the new computation (Table V).

2. Comparison of computations with experiments

Figures 19 and 20 show the results for the geometry with the asymmetrically confined cylinder. Velocities are normalized with the mean velocity U and stresses with $\tau_0 = 3\eta_0 U/R$ (= 127.3 Pa at the present flow rate).

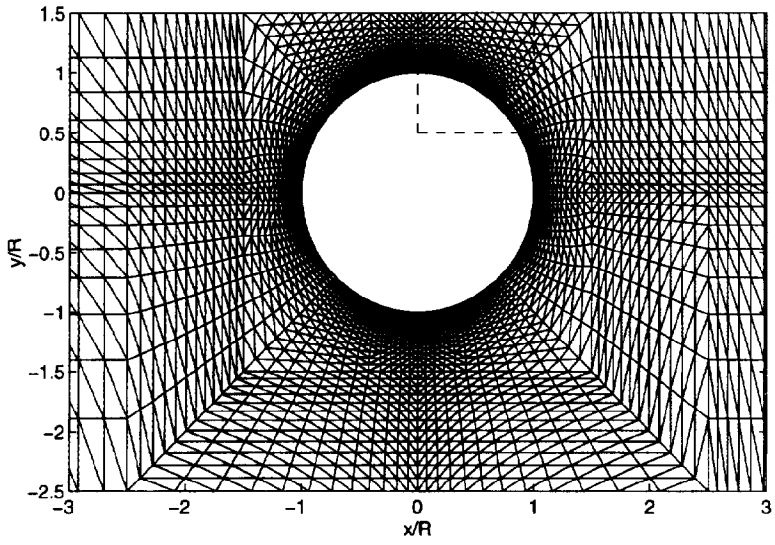

FIG. 17. Part of FEM mesh used for the geometry with asymmetrically confined cylinder.

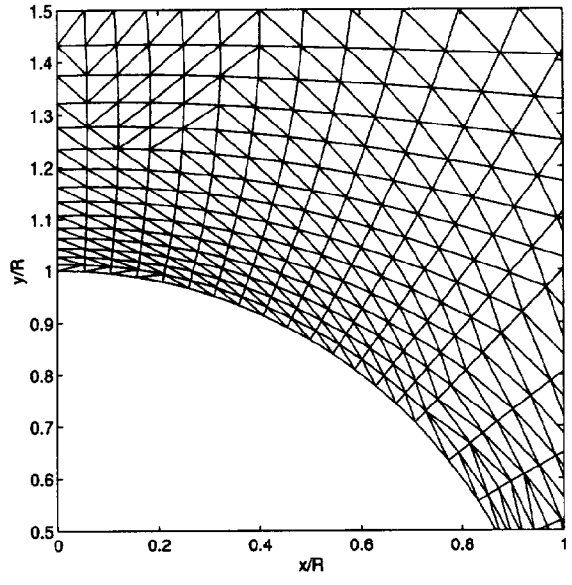

FIG. 18. Detail of FEM mesh used for the geometry with asymmetrically confined cylinder (the same region as marked with the dashed box in Fig. 17).

TABLE V. Mean velocity U and number of iterations n_{iter} for the computations with the four-mode PTT equation, in the case of the geometry with the asymmetrically confined cylinder. The solution with $U = 0.0868$ m/s was obtained by increasing the flow rate stepwise, which resulted in total 61 iterations.

U (m/s)	0.0212	0.0415	0.0562	0.0868
n_{iter}	13	15	12	21

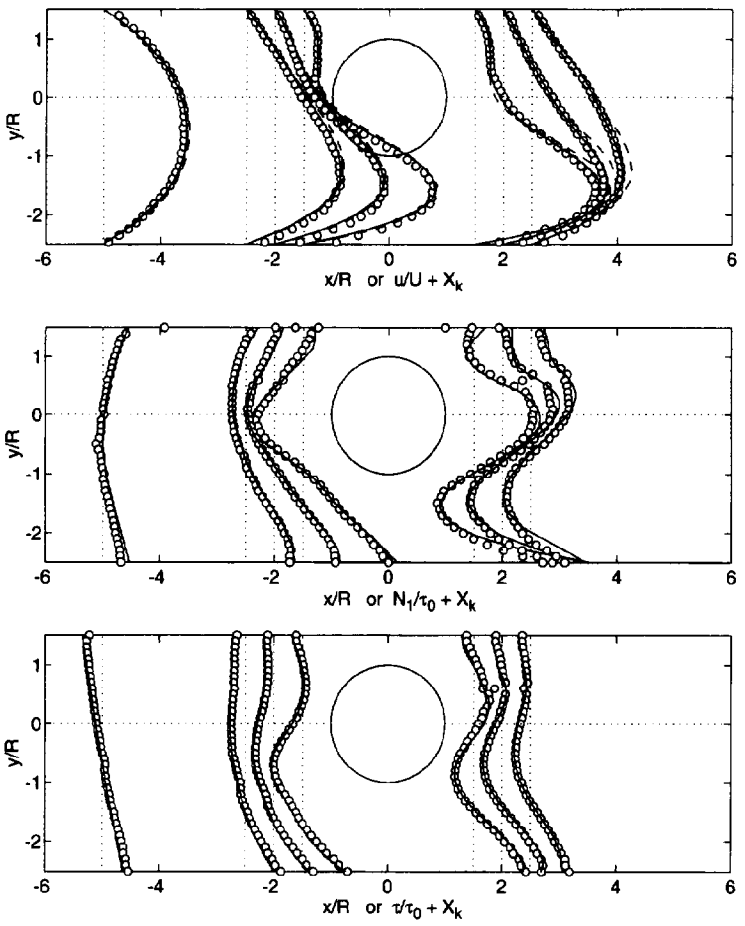

FIG. 19. Measured (○) and computed [(–) four-mode PTT, (– –) CY (velocities only)] quantities for the planar flow of the 5% PIB/C14 solution at De = 1.87 past an asymmetrically confined cylinder: velocity (top), first normal stress difference (middle), shear stress (bottom). Velocities are made dimensionless with the mean velocity U, and the stresses with τ_0, X_k denote the x/R coordinate of the base line corresponding with each separate curve (see text).

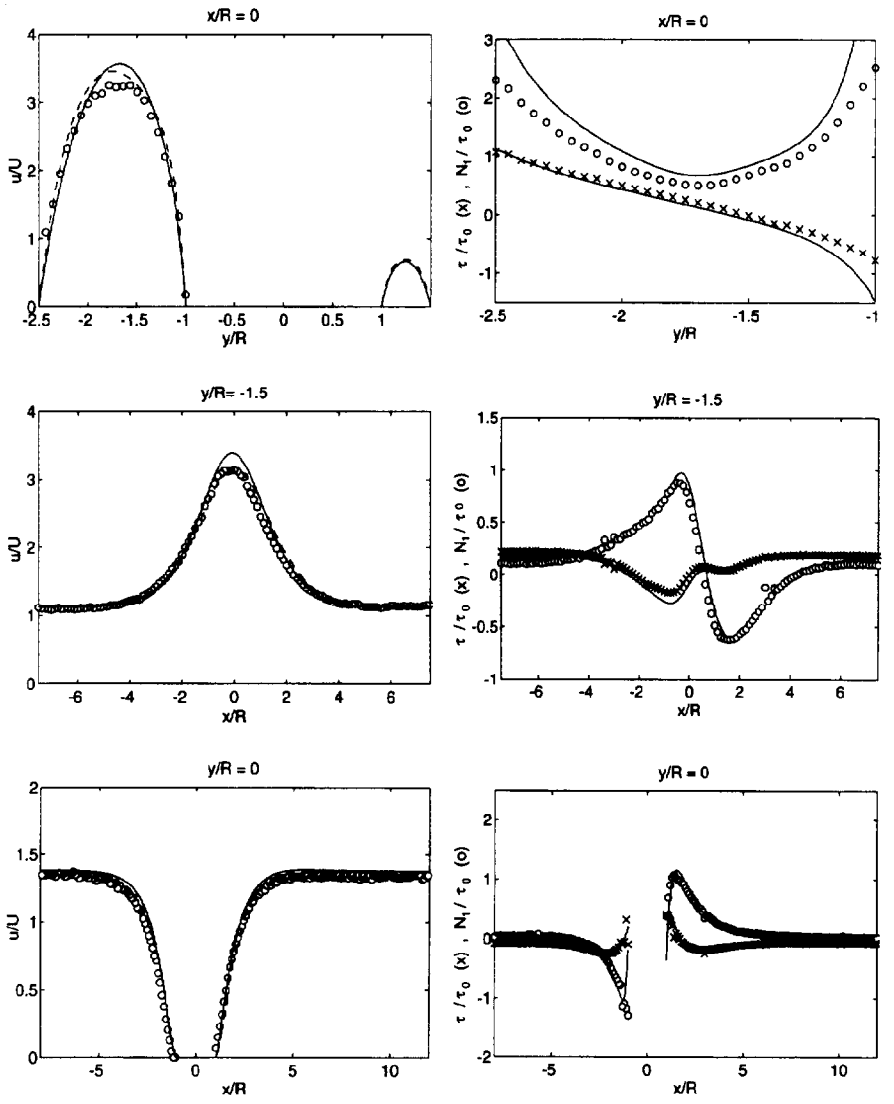

FIG. 20. Left column: measured (O) and computed velocities [(–) four-mode PTT, (– –) CY] along several lines in the flow of the 5% PIB/C14 solution past an asymmetrically confined cylinder. Right column: measured [(×): τ, (O): N_1] and computed stresses (four-mode PTT only) along the same lines as the velocities in the left column. De = 1.87.

For both constitutive equations, the four-mode PTT model and the generalized Newtonian model, the computed velocity profiles upstream of the cylinder agree well with those that were measured. Thus, the fluid is not sufficient elongation thickening to cause a significantly larger flow through the broader gap compared with an inelastic fluid. This correlates with the planar elongational viscosity as predicted by the four-mode PTT

model, which is nearly constant with elongation rate (Fig. 9). It appears that the shear thinning behavior is the dominant phenomenon for the velocity field in the present flow.

Comparison of the computed velocity profiles with the velocity measurements along line $x/R = 0$ in the broader gap shows that both models describe the measured velocity well (Fig. 20, top left plot). However, near the maximum of the profile, the CY model is closer to the measured data than the PTT model, which predicts a higher maximum. This might be due to too little shear thinning behavior of the PTT model for shear rates above 100 s^{-1}, since at this site high shear rates are present with a maximum value $\approx 250\ s^{-1}$ (compare Fig. 6).

The measured velocity profile along line $y/R = -1.5$ is described more accurately by the CY model than by the PTT model: the latter has too high a maximum (Fig. 20). For both models, the rising and descending parts of the computed velocity profile agree well with the measured data.

Along line $y/R = 0$ (upstream and downstream of the cylinder), excellent agreement is observed between both computed and measured velocities. No overshoot of the velocity downstream of the cylinder exists here.

Downstream of the cylinder, the computed velocity profiles for the PTT model agree excellently with the measured velocities and better than those for the CY equation (Fig. 19).

The normal stress differences along cross-sectional lines upstream of the cylinder as computed with the PTT model agree excellently with measured data. Downstream of the cylinder some small differences between computed and measured normal stress differences are found near the line $y/R = 0$, but the agreement is still impressive. Excellent point-wise agreement is found between measured and computed shear stresses at all sites (Fig. 19). Excellent agreement of computed and measured stresses exists along the line $y/R = 0$.

IV. DISCUSSION

Quinzani (1991) [see also Armstrong *et al.* (1992)] has shown that, out of six constitutive equations, the Phan-Thien–Tanner equation best describes the centerline stresses in the four to one contraction flow, followed by the Giesekus model. Though the Phan-Thien–Tanner model agreed best with measured data, still a fairly large difference was found between computed and measured results. Our present results give, for the Phan-Thien–Tanner model, a significantly closer agreement with experimental data in the confined flow around a cylinder. This difference in agreement is probably, or at least partly, caused by the integration procedure that Quinzani *et al.* used to compute stresses from measured velocities. Decoupling the kinematics from the stresses can lead to a solution that is inconsistent with the set of equations for the full flow problem. This problem is illustrated by the difference between the measured velocities along the downstream centerline and those computed with the finite element method for the single-mode PTT model (Fig. 14). Moreover, Baaijens (1993), who tested a new numerical method for viscoelastic flows, computed also Quinzani's contraction flow using the Phan-Thien–Tanner equation. He also found good agreement for the centerline stresses between the result of his (full) flow simulations and the measured stresses of Quinzani. Apparently, computation of the full flow field provides a more reliable route for testing constitutive equations.

The results of Baaijens (1993) with the PTT model also agree better with centerline stresses measured by Quinzani (1991) in the four to one contraction than the results of Mitsoulis (1993) with an integral model of the K-BKZ type.

With respect to the rheological behavior in elongational flows of the 5% PIB/C14 fluid, two observations suggest that the results of the computations for the flow past a cylinder correlate with the prediction of the steady state planar elongational viscosity (Fig. 9). First, only small differences exist between centerline stresses in the symmetric geometry for the one- and four-mode PTT fit and the four-mode Giesekus model [results of computations with this latter model can be found in Baaijens (1994)], similarly to their planar elongational viscosity curves. Second, in the asymmetric geometry there is no effect of elongational thickening that would cause the fluid to pass the cylinder preferably through the broader gap. This agrees with the nearly constant planar elongational viscosity curves $\eta(\dot{\epsilon})$ for these models.

On the other hand, the single-mode Giesekus model has a different elongational viscosity curve compared with the other three fits. It is likely that for this model fit the results of the centerline stresses past a symmetrically confined cylinder would differ from those for the other fits: it is expected to predict higher centerline stresses. Unfortunately, we did not obtain convergence of the finite element simulations with the one-mode Giesekus model fit. By integration of the constitutive equations along the centerline, using a polynomial fit of the measured velocities, we found indeed that the fitted single-mode Giesekus model predicts higher normal stresses. These results are plotted in Fig. 21. This figure also illustrates the inconsistency problem of the integration procedure that uses measured kinematics: a large difference exists between the results for the one-mode PTT model computed in this way and those computed with FEM.

The influence of the numerical method has also been investigated. Two other numerical methods have been used: the operator splitting method introduced by Baaijens (1993) and the discontinuous Galerkin method as discussed in Baaijens *et al.* (1994). Both methods agreed with the computations in this article within 5% [see Baaijens (1994)].

V. CONCLUSIONS AND RECOMMENDATIONS

In this study, the complex planar flow past a cylinder is used to evaluate in a rigorous way the viscoelastic constitutive equations of a polymeric liquid. The evaluation was made by comparing the results of finite element computations with point-wise measurements of both velocity and stress field. To facilitate the analysis and to connect with previous studies, a 5% (w/w) polyisobutylene solution in tetradecane was used as a model fluid. In the results, Deborah numbers range between 0.25 and 2.32 in the symmetrical geometry and it equalled 1.87 in the asymmetrical geometry.

The main conclusions and recommendations can be summarized as follows.

In the experimental arrangement developed in this study, accurate point-wise mappings of velocity and stress fields can be obtained, using simultaneously laser Doppler anemometry and a flow-induced birefringence technique based on polarization modulation. Together, these two experimental techniques constitute useful tools to obtain experimental data that are suitable for testing constitutive equations rigorously by a quantitative comparison with numerical flow simulations.

In the experiments stable, nominally two-dimensional flows were established, while retaining for the fluid used constant material functions in simple shear flow.

There is confidence that the results for the viscoelastic constitutive equations present accurate solutions of the mathematical problem and were not influenced by the numerical method used, since they agreed well with those for two other widely varying numerical techniques.

Good (to excellent) agreement was obtained between experiments and finite element computations for the planar flows using the four-mode PTT model. The agreement is

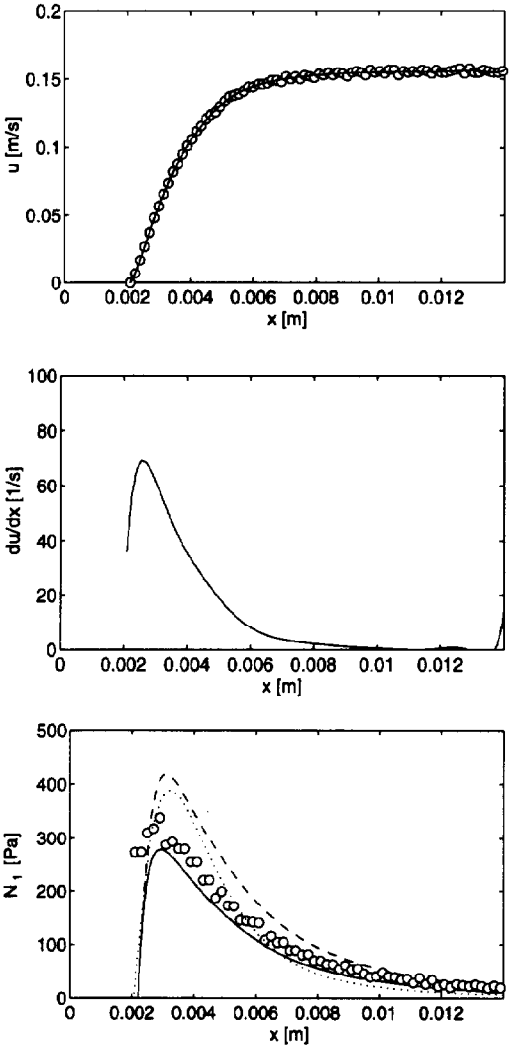

FIG. 21. Computation of normal stress difference along centerline by integration of constitutive equations with the use of measured velocity field. Top: centerline velocities downstream of cylinder with polynomial fit. Middle: derivative of velocity fit. Bottom: predictions of normal stress difference along centerline: single-mode PTT model (–), single-mode Giesekus model (– –), result for finite element computation with single mode PTT model (···), experimental data (○).

satisfying, particularly since this study is the first that successfully compared point-wise velocity and stress measurements with viscoelastic simulations in a more or less complex flow. This result is probably due to the absence of singularities like those present in abrupt contraction flows.

A generalized Newtonian model describes details of the velocity field even more accurately, but fails with the prediction of normal stresses.

It appears that the model fluid used is not very sensitive for elongational deformation, i.e., its elongational viscosity depends only weakly on elongational rate. This is also

predicted by the four-mode PTT and Giesekus models which are fitted adequately with data measured in simple shear flow. The use of a model fluid that is more sensitive for elongational flows will give more drastic viscoelastic effects, see for example the results of Walters and co-workers with polyacrylamide solutions [Dhahir and Walters (1989), Cochrane *et al.* (1981), Jones and Walters (1989), Georgiou *et al.* (1991)].

The integration procedure to compute stresses that uses measured kinematics can lead to inaccurate results because the method is not self-consistent.

Our previous results, reported in Baaijens *et al.* (1994), disagree with the results in this article. It is most likely that this is caused by a change in the rheological properties in the fluid during the former experiments. Unfortunately, we did not succeed in identifying the real cause, since we were not able to reproduce the precise effect.

Extension to the analysis of the transient rheological behavior of the fluid during start-up of the flow around the cylinder is promising as a more rigorous test for constitutive models.

In future work on polymer solutions it is recommended, besides using higher Deborah numbers, that one search for a flow situation where normal stresses have a more pronounced influence on the velocity field, since then the flow is expected to discriminate more strongly between different models.

ACKNOWLEDGMENTS

We gratefully acknowledge Professor Gerald G. Fuller (Stanford University), whose advise on rheo-optics and cooperation have been invaluable. We thank Theo van Duppen, Toon van Gils, and Sjef Garenfeld for constructing parts of the experimental apparatus and Joris van Dam, Jeroen Schoonen, and particularly Peter Kruijt for their contributions to the experiments.

References

Aldhouse, S. T. E., M. R. Mackley, and I. P. T. Moore, "Experimental and linear viscoelastic stress distribution measurements of high density polyethylene flowing into and within a slit," J. Non-Newt. Fluid Mech. **21**, 359–376 (1986).

Armstrong, R. C., R. A. Brown, L. M. Quinzani, G. H. McKinley, and J. A. Byars, "Measurement of velocity and stress fields in complex polymer flows," in *Proc. XI Int. Cong. Rheology, Theoretical and Applied Rheology, Brussels*, edited by P. Moldenaers and R. Keunings (Elsevier, Amsterdam, 1992), pp. 16–23.

Baaijens, F. P. T., "Numerical analysis of start-up planar and axisymmetric contraction flows using multi-mode differential constitutive models," J. Non-Newt. Fluid Mech. **48**, 147–180 (1993).

Baaijens, F. P. T., J. P. W. Baaijens, G. W. M. Peters, and H. E. H. Meijer, "A numerical and experimental investigation of viscoelastic flow around a cylinder," J. Rheol. **38**, 351–376 (1994).

Baaijens, J. P. W., "Evaluation of constitutive equations for polymer melts and solutions in complex flows," Ph.D. thesis, Eindhoven University of Technology, The Netherlands (1994).

Bird, R. B., C. F. Curtiss, R. C. Armstrong, and O. Hassager, *Dynamics of Polymeric Liquids* (Wiley, New York, 1987).

Boger, D. V., "Viscoelastic flow through abrupt contractions," Annu. Rev. Fluid Mech. **19**, 157–182 (1987).

Brown, R. A. and G. H. McKinley, "Report on the VIIIth int. workshop on numerical methods in viscoelastic flows," J. Non-Newt. Fluid Mech. **52**, 407–413 (1994).

Cochrane, T., K. Walters, and M. F. Webster, "On Newtonian and non-Newtonian flow in complex geometries," Philos. Trans. R. Soc. London A. **301**, 163–181 (1981).

Cuvelier, C., A. Segal, and A. A. van Steenhoven, *Finite Element Methods and Navier–Stokes Equations* (D. Reidel, Dordrecht, 1986).

Davidson, D. L., W. W. Graessley, and W. R. Schowalter, "Velocity and stress fields of polymeric liquids flowing in a periodically constricted channel: Experimental methods and straight channel validations," J. Non-Newt. Fluid Mech. **49**, 317–344 (1993a).

Davidson, D. L., W. W. Graessley, and W. R. Schowalter, "Velocity and stress fields of polymeric liquids flowing in a periodically constricted channel: Observations of non-Newtonian behavior," J. Non-Newt. Fluid Mech. **49**, 317–344 (1993b).

Dhahir, S. A. and K. Walters, "On Non-Newtonian flow past a cylinder in a confined flow," J. Rheol. **33** (6), 781–804 (1989).

Drain, L. E., *The Laser Doppler Technique* (Wiley, Chicester, 1980).

Ferry, J. D., *Viscoelastic Properties of Polymers*, 3rd ed. (Wiley, New York, 1980).

Fuller, G. G., "Optical rheometry," Annu. Rev. Fluid Mech. **22**, 387–417 (1990).

Fuller, G. G., *Measurement of Dynamics and Structure in Complex Liquids: Theory and Practice of Optical Rheometry* (Oxford University Press, Oxford, 1995).

Fuller, G. G. and K. J. Mikkelsen, "Note: Optical rheometry using a rotary polarization modulator," J. Rheol. **33**, 761–769 (1989).

Galante, S. R. and P. L. Fratini, "Spatially resolved birefringence studies of planar entry flow," J. Non-Newt. Fluid Mech. **47**, 289–337 (1993).

Georgiou, G., S. Momani, M. J. Crochet, and K. Walters, "Newtonian and non-Newtonian flow in a channel obstructed by an antisymmetric array of cylinders," J. Non-Newt. Fluid Mech. **40**, 231–260 (1991).

Han, C. D. and L. H. Drexler, "Studies of converging flows of viscoelastic polymeric melts. I. Stress-birefringent measurements in the entrance region of a sharp-edged slit die," J. Appl. Polym. Sci. **17**, 2329–2354 (1973a).

Han, C. D. and L. H. Drexler, "Studies of converging flows of viscoelastic polymeric melts. II. Velocity measurements in the entrance region of a sharp-edged slit die," J. Appl. Polym. Sci. **17**, 2355–2368 (1973b).

Han, C. D. and L. H. Drexler, "Studies of converging flows of viscoelastic polymeric melts. III. Stress and velocity distributions in the entrance region of a sharp-edged slit die," J. Appl. Polym. Sci. **17**, 2369–2393 (1973c).

Hulsen, M. A., "Analysis and numerical simulation of the flow of viscoelastic fluids," Ph.D. thesis, Delft University of Technology, The Netherlands (1988).

Hulsen, M. A., "A numerical method for solving steady $2d$ and axisymmetrical viscoelastic flow problems with an application to inertia effects in contraction flows," Research note MEMT 11, Delft University of Technology, The Netherlands (1990).

Hulsen, M. A. and J. van der Zanden, "Numerical simulation of contraction flows using a multi-mode Giesekus model," J. Non-Newt. Fluid Mech. **38**, 183–221 (1991).

Isayev, A. I. and R. K. Upadhyay, "Two-dimensional visco-elastic flows: Experimentation and modeling," J. Non-Newt. Fluid Mech. **19**, 135–160 (1985).

Jones, D. M. and K. Walters, "The behavior of polymer solutions in extension dominated flows, with applications to enhanced oil recovery," Rheol. Acta **28**, 482–498 (1989).

Kajiwara, T., S. Ninomiya, Y. Kuwano, and K. Funatsu, "Numerical simulation of converging flow of polymer melts through a tapered slit die," J. Non-Newt. Fluid Mech. **48**, 111–124 (1993).

Kiriakidis, D. G., H. J. Park, E. Mitsoulis, B. Vergnes, and J. F. Agassant, "A study of stress distribution in contraction flows of an LLDPE melt," J. Non-Newt. Fluid Mech. **47**, 339–356 (1993).

Larson, R. G., *Constitutive Equations for Polymer Melts and Solutions* (Buttersworth, Boston, 1988).

Liu, Y. J., J. Nelson, J. Feng, and D. D. Joseph, "Anomalous rolling of spheres down an inclined plane," J. Non-Newt. Fluid Mech. (to be published, 1995).

Macosko, C. W., *Rheology: Principles, Measurements, and Applications* (VCH, New York, 1994).

Maders, H., B. Vergnes, Y. Demay, and F. Agassant, "Steady flow of a White–Metzner fluid in a $2D$ abrupt contraction: Computation and experiments," J. Non-Newt. Fluid Mech. **45**, 63–80 (1992).

Manero, O. and B. Mena, "On the slow flow of viscoelastic liquids past a circular cylinder," J. Non-Newt. Fluid Mech. **9**, 379–387 (1981).

McKinley, G. H., "Dynamics of polymer solutions," Ph.D. thesis, Massachusetts Institute of Technology, Cambridge (1991).

Mena, B. and B. Caswell, "Slow flow of an elastic-viscous fluid past an immersed body," Chem. Eng. J. **8**, 125–134 (1974).

Mitsoulis, E., "Numerical simulation of planar entry flow for a polyisobutylene solution using an integral constitutive equation," J. Rheol. **37**, 1029–1040 (1993).

Olsson, T., "A solver for time dependent viscoelastic fluid flows," J. Non-Newt. Fluid Mech. **51**, 309–340 (1994).

Pilate, G. and M. J. Crochet, "Plane flow of a second-order fluid past submerged boundaries," J. Non-Newt. Fluid Mech. **2**, 323–341 (1977).

Quinzani, L. M., Birefringence studies of entry flows of concentrated polymer solutions, Ph.D. thesis, Massachusetts Institute of Technology, Cambridge (1991).

Quinzani, L. M., G. H. McKinley, R. C. Armstrong, and R. A. Brown, "Modelling the rheology of polyisobutylene solutions," J. Rheol. **34**, 705–749 (1990).

Quinzani, L. M., R. C. Armstrong, and R. A. Brown, "Birefringence and laser-Doppler velocimetry (LDV) studies of viscoelastic flow through a planar contraction," J. Non-Newt. Fluid Mech. **52**, 1–36 (1994).

Raiford, W. P., L. M. Quinzani, P. J. Coates, R. C. Armstrong, and R. A. Brown, "LDV measurements of viscoelastic flow transitions in abrupt axisymmetric contractions: Interaction of inertia and elasticity," J. Non-Newt. Fluid Mech. **32**, 39–68 (1989).

Rajagopalan, D., J. A. Bryars, and R. C. Armstrong, "Comparison of numerical simulations and birefringence measurements in viscoelastic flow between eccentric rotating cylinders," J. Rheol. **36** (7), 1349–1375 (1992).

Schoonen, J., Eindhoven University of Technology, The Netherlands, private communication (1994).

Segal, A., *Manual SEPRAN package* (Ingenieursburo SEPRA, Leidschendam, The Netherlands, 1992).

Townsend, P., "A numerical simulation of Newtonian and visco-elastic flow past stationary and rotating cylinders," J. Non-Newt. Fluid Mech. **6**, 219–243 (1980).

Ultmann, J. S. and M. M. Denn, "Slow viscoelastic flow past submerged objects," Chem. Eng. J. **2**, 81–89 (1970).

Walters, K., "Recent developments in rheometry," in *Proc. XI Int. Cong. Rheology, Theoretical and Applied Rheology, Brussels* (Elsevier, Amsterdam, 1992).

White, S. A. and D. G. Baird, "Flow visualization and birefringence studies on planar entry flow behavior of polymer melts," J. Non-Newt. Fluid Mech. **29**, 245–267 (1988).

Zoetelief, W., "On the numerical simulation of the multilayer injection moulding process," Technical Report WFW 92.100, Eindhoven University of Technology, The Netherlands (1992).